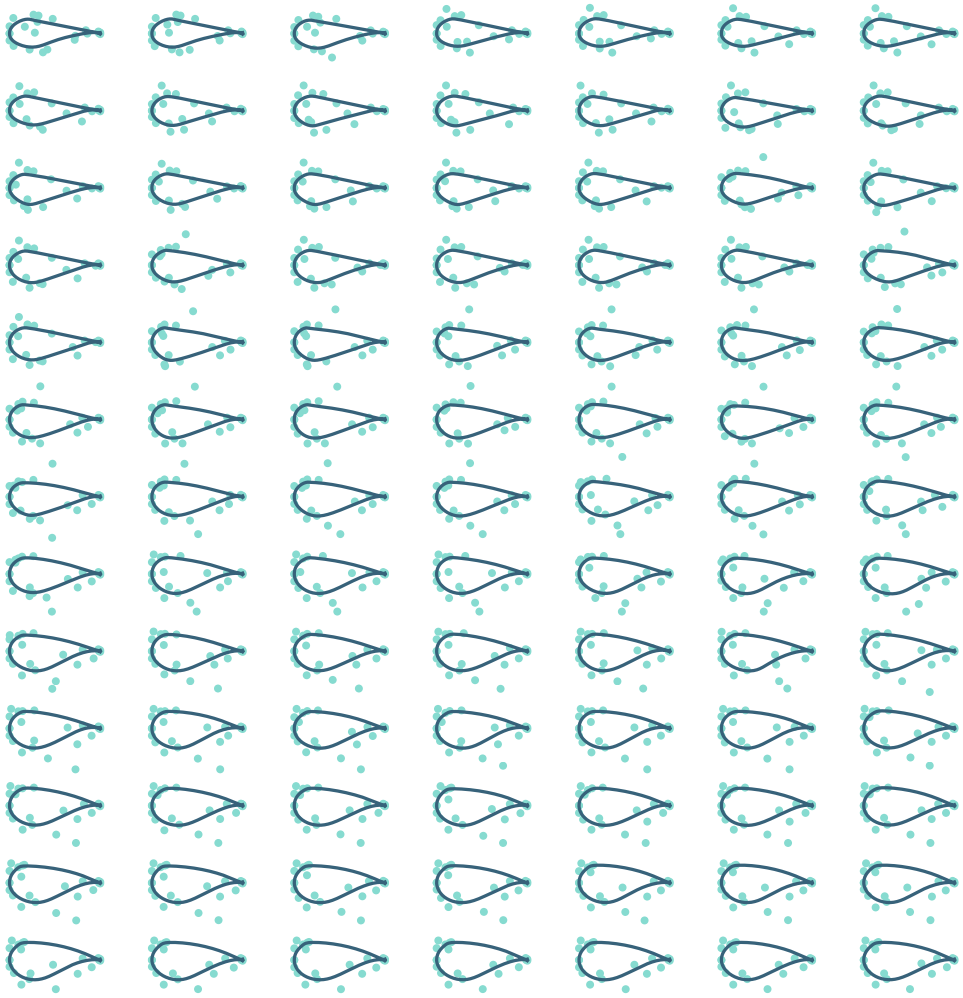

Design and optimization of airfoil profiles for vertical axis wind turbines

Master's thesis in Applied Mechanics

JOHANNA STENMARK

DEPARTMENT OF MECHANICS AND MARITIME SCIENCES
CHALMERS UNIVERSITY OF TECHNOLOGY
Gothenburg, Sweden 2023
www.chalmers.se

Master's thesis 2023

Design and optimization of airfoil profiles for vertical axis wind turbines

JOHANNA STENMARK

CHALMERS
UNIVERSITY OF TECHNOLOGY

Department of Mechanics and Maritime Sciences
Division of Fluid dynamics
Chalmers University of Technology
Gothenburg, Sweden 2023

Design and optimization of airfoil profiles for vertical axis wind turbines
JOHANNA STENMARK

Supervisor: Rémi Corniglion, SeaTwirl
Examiner: Håkan Nilsson, Mechanics and Maritime Sciences

Master's Thesis 2023
Department of Mechanics and Maritime Sciences
Division of Fluid dynamics
Chalmers University of Technology
SE-412 96 Gothenburg
Telephone +46 31 772 1000

Cover: Optimized family of airfoils with regards to section modulus and power coefficient obtained using the genetic algorithm NSGA-II in Python.

Typeset in LaTeX
Gothenburg, Sweden 2023

Design and optimization of airfoil profiles for vertical axis wind turbines
JOHANNA STENMARK
Department of Mechanics and Maritime Sciences

Chalmers University of Technology

Abstract

Offshore floating vertical axis wind turbines could be a great renewable energy source to meet the needs for renewable energy since they can be placed in deep waters and unlock new potential areas for wind farms. The specific operating conditions of a vertical axis wind turbine blade call for a purposely designed airfoil profile to improve performance and reduce cost. The blades must be both aerodynamically and structurally good. Airfoil profiles were optimized using a genetic algorithm with both an aerodynamic and structural objective: to maximize the power coefficient and to maximize the section modulus. The power coefficient was calculated with the actuator cylinder method using polars from XFoil which captured the operating conditions of the vertical axis wind turbine. The obtained optimized family of airfoils showed increased blade and turbine performance compared to the often used NACA 0018. Some of the optimized airfoil profile have the potential to reduce the weight of vertical axis wind blades based on a simple estimation.

Keywords: VAWT, bi-objective optimization, genetic algorithm, NSGA-II, airfoil profile, AC method, renewable energy

Acknowledgements

I would like to thank my supervisor Rémi Corniglion for his support, helpful insights and suggestions on what to do to improve the thesis. Thanks to his insight in the problem at hand and thought out suggestion for the methods in order to achieve the aim of this thesis, the work with the thesis ran smoothly. I would also like to thank Karl Arvidsson for the help with understanding the impact of the section modulus for the blades. As well as the other people at SeaTwirl that has supported my work during this thesis. I also wish to thank my examiner Håkan Nilsson for his feedback and help.

Johanna Stenmark, Gothenburg, June 2023

List of Acronyms

Below is the list of acronyms that have been used throughout this thesis listed in alphabetical order:

AC	Actuator cylinder
GA	Genetic algorithm
HAWT	Horizontal axis wind turbine
TSR	Tip speed ratio
VAWT	Vertical axis wind turbine

Nomenclature

Below is the nomenclature of parameters, and variables that have been used throughout this thesis.

Variables

c	Chord of airfoil
C_d	Drag coefficient
C_l	Lift coefficient
C_P	Power coefficient
C_T	Thrust coefficient
t	Thickness of airfoil
U	Relative or inflow wind
U_∞	Free-stream velocity
v	Induced velocity
w	Section modulus
α	Angle of attack
σ	Solidity
λ	Tip speed ratio
θ	Azimuth angle
ρ	Density

Parameters

N	Number of individuals in a generation
p_c	Cross-over probability
p_m	Mutation probability

Contents

List of Figures

List of Tables

1
Introduction

There are many different options for renewable energy sources, one such source is wind power. This thesis will focus on a floating vertical axis wind turbine.

1.1 Background

With an increasing global temperature due to climate change there is a challenge for the energy sector: how to sustain the growing global energy needs without further contributing to climate change. The renewable energy sources must be able to replace current non-renewable sources and also be able to grow with the increasing energy demand. There are many possible sources for renewable energy with a lot of potential. Even though there globally is a huge potential use of renewable energies there is still only a minor part that is being utilized [1].

One source of renewable energy is wind power which harnesses the kinetic energy of the wind and converts it into electric energy using a wind turbine. Wind energy also has the potential to be placed offshore which opens up vast possible areas for wind farms. When placed offshore it is also possible to have floating wind turbines which can be placed at locations with deeper water depth. Wind turbines are divided into two categories based on the axis of rotation: horizontal axis wind turbines (HAWT) and vertical axis wind turbines (VAWT). Due to difference in rotation axis the HAWT and VAWT operate at very different conditions and thus the aerodynamics of them are also substantially different. During operation the blades, and the whole turbine, is subjected to aerodynamic forces which will be different depending on the type of turbine since they have different aerodynamics [2]. In order for wind turbines to be an attractive solution to other energy sources they need to be designed to be able to extract as much energy from the wind as possible, they need to be aerodynamically optimal. On the other hand the turbine, and what is of most interest for this thesis, the blades need be in operation for some time before being replaced. They must therefore be able to withstand the forces that act on it during operation, it must be structurally optimal to avoid wasting material and having unnecessary weight.

Each type of wind turbine comes with its own advantages and disadvantages. The VAWT has the advantage of being omni-directional, meaning it is insensitive to wind direction, and can have a simpler design since there is no requirement for a yawing system. Another benefit of the VAWT compared to the HAWT is the po-

tential of scaling up the size of the turbine [3]. While some disadvantages are that not all of the blade will contribute to production at the same time which lowers the effectivity of the VAWT. Traditionally, HAWT has been used and therefore a lot more research for eg wind farm layout and design optimization has been done. Since HAWT and VAWT operate very differently the development done for HAWT is not directly applicable for a VAWT. In recent years there have been an increasing interest for VAWT and studies specifically for VAWT parameters have been made [2].

1.1.1 SeaTwirl's VAWT

It is lift-driven, floating and built to be used in offshore wind farms. The turbine is a H-rotor Darrieus which means that the blades are straight for their whole length and parallel to the tower. The design is similar to the floating VAWT in figure 1.1. The blades are connected to the tower by the struts and the tower is connected to a structure that consists of a floating element and a spar located below the water surface. The spar functions the same as a keel for a boat: it stabilises the whole structure and prevents it from tipping over. The wind turbine is not bottom-fixed but is instead secured using mooring lines. This gives a larger range of possible locations for the VAWT since it can be placed were the water depth is too deep for a bottom fixed version. The cross-section of the blades are called an airfoil and finding a shape that works optimally for the VAWT can greatly benefit its performance.

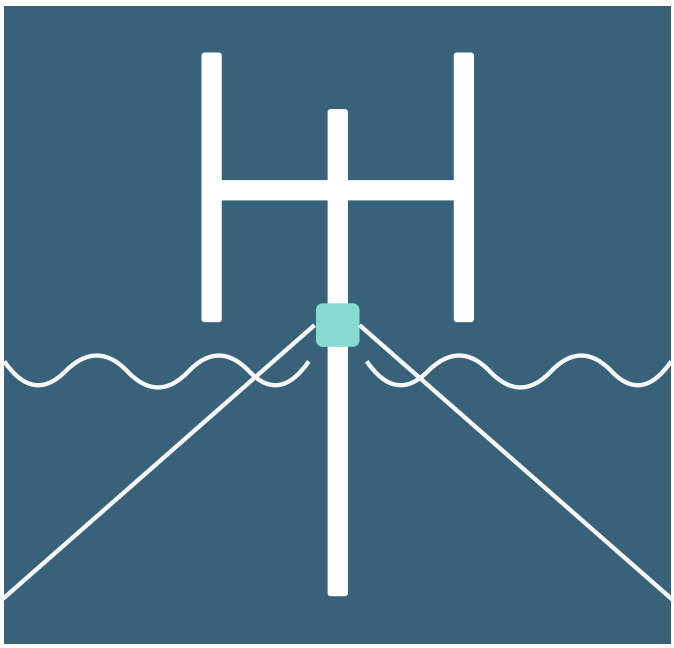

Figure 1.1: A simplified visualisation of a floating VAWT.

1.1.2 Existing works on VAWT airfoil profiles

Aiming to optimize the VAWT performance by changing the blade profiles have been made but while the results are interesting they are not directly applicable. Blades have been optimized with regards to aerodynamic performance [4] not having a structural objective gives airfoils that might not be able to withstand the acting forces. The VAWT can operate at different conditions which can greatly impact which range it operates optimally in. In the studies by Ferreira and Guerts [5] and Kemp [6] the operating range it is optimized for makes it too limited.

1.2 Aim

In order to improve the performance of the VAWT it is of great interest to find an optimal airfoil profile that is specific for VAWT's since as stated before they operate better at different conditions compared to HAWT's. Therefore a family of airfoil profiles both aerodynamically and structurally optimal for VAWT's is sought. The aerodynamic performance will be set to the power coefficient C_P and the structural performance is set to be the section modulus w. These aims are competing against each other with regards to the design of the airfoil. An aerodynamically good airfoil is usually thin while a structurally good airfoil is usually thick. The following statement will be the goal for this thesis

- The optimized family of airfoils for a VAWT along a Pareto curve for a 2D airfoil profile with regards to the section modulus and the power coefficient.

1.3 Limitations

A single isolated VAWT blade has been considered. Any change in the wind and possible wakes from adjacent turbines or blades in any direction has not been considered.

The simulations have only been run in 2D and not 3D. No 3D effects will be taken into account such as the shape or length of the blade in the spanwise direction, what happens at the tip of the blades or the stall angle of attack. The simulations are also run for an idealized case where no strut losses or 3D losses are considered which will impact the calculated performance of the turbine.

Since the VAWT is floating it will therefore sometimes tilt due to the wind and waves thus creating an angle between the incoming flow and the blades. For the optimization it is assumed that this angle is set to zero.

Since only SeaTwirl's VAWT is of interest no other types of VAWT is considered and any impact in performance from change in curvature of the blade or a varying cross section is not studied.

2
Theory

A few important concepts and theory that is good to grasp are presented in the following sections. Starting with airfoils, VAWT, parameterization, optimization and finally the software used.

2.1 Airfoil

The cross section of the turbine blade is called an airfoil and its geometric shape has a great impact on its aerodynamic performance. An airfoil has specific terms that describe its geometric properties and the flow field around the airfoil impacts how its aerodynamic performance is. The airfoil is usually represented by a set of data points for its x and y-coordinates.

2.1.1 Geometric parameters

The front and back is called the leading and trailing edge respectively with the chord line going straight between them. The length of the chord line is called the chord, c. An airfoil might be symmetrical around the chord line or it might be unsymmetrical and is then called a cambered airfoil. For a cambered airfoil, such as the one in figure 2.1, the airfoils neutral line that runs halfway between its upper and lower surface is called the camber line. For a symmetrical airfoil the neutral line is the chord line.

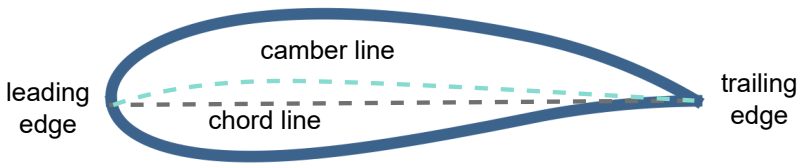

Figure 2.1: Schematics of a cambered airfoil with the location of the relevant terms trailing edge, leading edge, chord line and camber line shown.

An airfoil is usually described with its length and thickness normalized to its chord. The thickness, t/c is taken as the thickest part between the top and bottom of the airfoil. The trailing edge of the airfoil is often shown as pointy but this is

very difficult to achieved when manufacturing an airfoil and should be taken into consideration.

2.1.2 Aerodynamic parameters

When the airfoil moves through the flow field it is subjected to a resulting force that is due to pressure and friction from the flow. The resulting force is usually divided into a lift component that is normal to the flow direction and a drag component that is tangent to the flow direction. Lift and drag is usually quantified with the lift coefficient C_l and drag coefficient C_d respectively.

The angle between the relative or inflow wind and the chord line is called the angle of attack, α, and greatly impacts the airfoils performance since the lift and drag force is dependent on the direction of the flow hitting the blade. The black arrow in figure 2.2 shows the direction of the inflow wind compared to the chord line and the resulting angle of attack as well as the direction of the forces on the airfoil. The angle of attack shown is positive and if the airfoil was hit on the other side of the chord line it would be a negative angle of attack with a lift force pointing downward, it would generate negative lift. Note that a symmetrical airfoil generates zero lift at zero angle of attack [7] and a camber increases the lift of the airfoil.

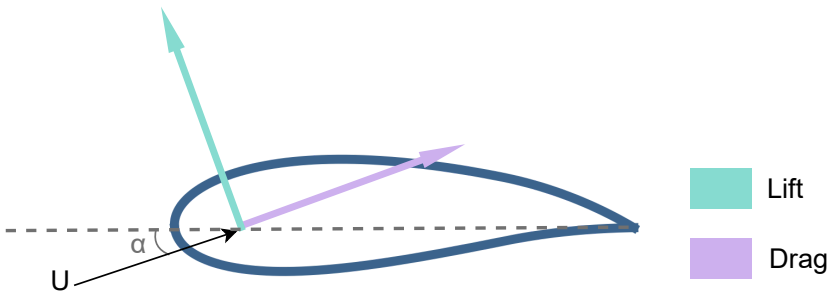

Figure 2.2: The lift and drag forces, the velocity U and the angle of attack α for a cambered airfoil.

As the angle of attack increases the lift increases. This holds only up until a certain angle of attack where the flow can no longer follow the curvature of the airfoil and separation starts to occur which creates a sudden drop in lift as in figure 2.3. This is called stall and could occur very drastically. At which angle of attack stall occurs depends on the airfoil geometry and the flow conditions so it does not always happen at the same angle of attack.

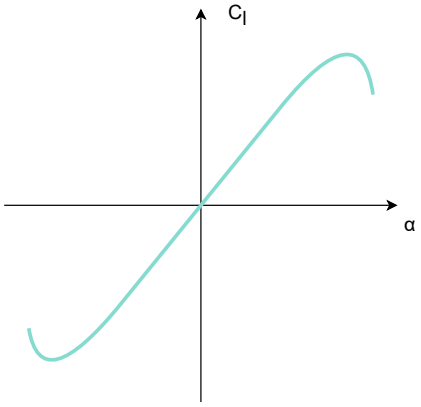

Figure 2.3: Change in lift coefficient as a function of angle of attack for an arbitrary symmetrical airfoil. The sharp drops in lift after a peak lift coefficient has been reached at the edges is due to stall.

A non-dimensional number often used within fluid dynamics is the Reynolds number. It describes the characteristics of conditions of the flow. It is a ratio of inertial forces to viscous forces and defined for an airfoil as

$$Re = \frac{\rho U_\infty c}{\mu}, \tag{2.1}$$

where μ is the fluid dynamic viscosity. The Reynolds number greatly impacts the performance of an airfoil. A lower Reynolds number means that the effects from viscous forces increase more relatively to inertial effects and the surface friction affects the airfoil more. This in turn changes the velocity, the pressure gradient over the airfoil and the lift and drag [8].

2.2 Vertical axis wind turbines

There are various designs of VAWT with different number of blades, usually between 2 and 4, different number of struts and different curvature of the blades ranging from straight to curved. Due to the VAWT rotating with a vertical axis there are a few concepts that greatly impact specifically the design of a VAWT. As well as parameters that are important to its performance.

Two important parameters are tip speed ratio, TSR or λ, and the solidity, σ. TSR is the ratio between the rotational velocity of the blades and the free flow velocity and greatly impacts the performance of the VAWT. It is defined as

$$\lambda = \frac{\Omega R}{U_\infty}, \tag{2.2}$$

where Ω is the angular velocity, R is the radius of rotation and U_∞ is the free stream velocity. Since the blades for the VAWT in question are straight, the whole blade has the same TSR. The solidity σ of the turbine which is the ratio of the area of

the blades over the total swept area of the blades. SeaTwirl defines the solidity according to

$$\sigma = \frac{nb \cdot c}{2R}, \tag{2.3}$$

with the number of blades, nb, and the radius R.

The axis of a VAWT is perpendicular to the flow which creates an upwind and a downwind half of rotation as seen in figure 2.4. The azimuth angle θ denotes the azimuthal position of a blade during the rotation and the upwind and downwind region changes at $\theta = 0°$ and $\theta = 180°$. When a blade is in the upwind region it extracts energy from the undisturbed free stream flow that hits the outside of the blade which gives resulting forces acting inward towards the tower. In the downwind region the now disturbed flow hits the inside of the blade but the resulting forces are still acting in the same direction which is now outwards. As the blade rotates the angle of attack of the flow over the airfoil varies with azimuth angle. This in turn gives a difference in the lift and drag forces during the rotation.

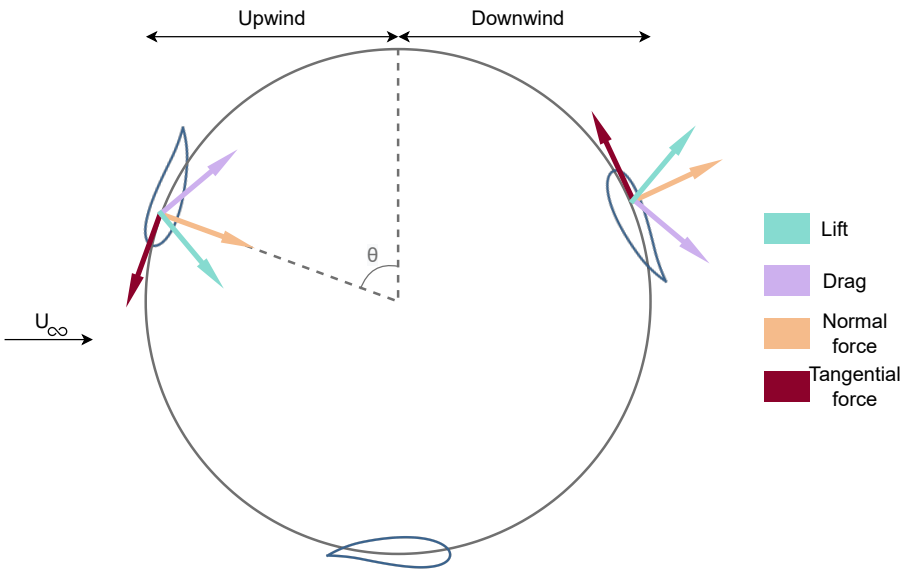

Figure 2.4: Schematic of the VAWT seen from above with free stream velocity of U_∞. The blade forces, shown as unit vectors, for the upwind ($0 < \theta < 180°$) and downwind ($180° < \theta < 360°$) part of the rotation are shown.

Note that during a rotation the angle of attack goes from positive to negative at $\theta = 180°$ and $\theta = 0°$ which impacts the design of the blade. The angle of attack is both positive and negative during operation which is a major difference compared to a HAWT and why a blade profile optimized for a HAWT does not work optimally for a VAWT.

The angle of attack varies with θ as well as the TSR. The angle of attack is defined, as stated, between the chord line and the relative inflow wind which in this

case is the relative flow between the free stream velocity, U_∞ and the velocity of the blade due to rotation. If only the tangential velocity of the blade is altered then how the angle of attack varies depending on the azimuth angle for different TSR is shown in figure 2.5. The angle of attack is lower with increasing TSR due to the increase in tangential blade velocity. The lower amplitude for $\theta > 180°$ is due to the lowered flow velocity after some energy has been extracted by the blade in the upwind region.

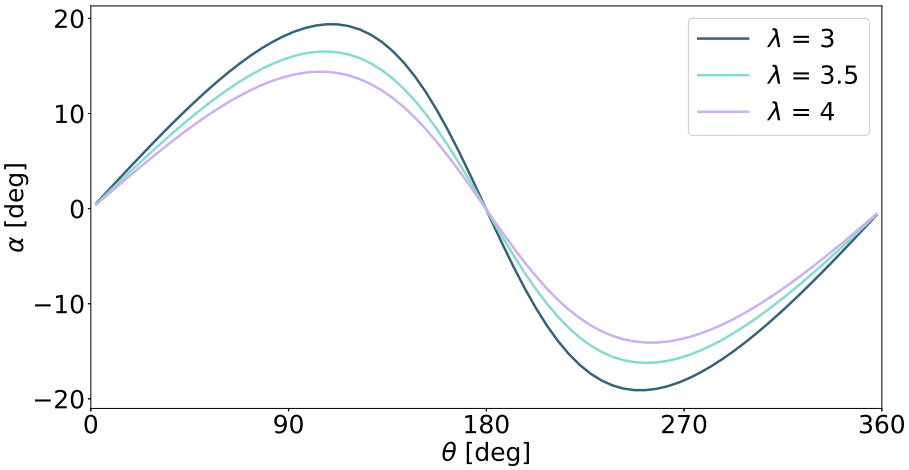

Figure 2.5: Variation of the angle of attack for the airfoil NACA 0018 for different TSR, obtained by only changing the tangential velocity of the blade, during a full rotation of the turbine. Obtained with the AC method presented in section 2.2.2.1.

Since the blade is experiencing both positive and negative angle of attacks, the blade forces acting on the blade are different between the upwind and downwind region as seen in figure 2.4. The lift force is acting both normal to the outside and inside of the blade which means that for a VAWT the camber of the airfoil can potentially be on either side. Due to positive angle of attack for the upwind part a concave curve on the outside, as in figure 2.4, is more beneficial and the opposite for the downwind part. The placement depends on whether more energy should be extracted from the undisturbed flow during the upwind part or try to make the two halves perform more equally by increasing the energy that can be extracted during the downwind half. The forces acting on the blade also bends the blades and therefore it is very important to have blades with both good aerodynamical and structural properties.

2.2.1 Section modulus

For the structural optimization the section modulus w is chosen. It is a geometric property that gives a measurement of how well a cross-section can withstand bending for a certain moment. It is usually used when calculating properties for beams but can also be used for other geometries that need to withstand bending. With a higher value of w then the airfoil, in this case, can withstand higher loads. It is calculated

according to

$$w = \frac{I_{xx}}{y} = \frac{M}{\sigma_w}, \tag{2.4}$$

I_{xx} is the second moment of inertia around the x-axis, y is the maximum thickness of the airfoil taken from the neutral axis and M is the moment acting on the blades over the stress σ_w, on the blades. This means that the second moment of inertia is normalized to the thickness of the airfoil and should limit that simply a thicker airfoil performs better. The equation for obtaining I_{xx} was taken from a MIT course [9] and calculated as

$$\begin{aligned} A &= \int_0^c [Z_u - Z_l]dx \\ \bar{z} &= \frac{1}{A}\int_0^c \frac{1}{2}[Z_u^2 - Z_l^2]dx \\ I &= \int_0^c \frac{1}{3}[(Z_u - \bar{z})^3 - (Z_l - \bar{z})^3]dx. \end{aligned} \tag{2.5}$$

Here, A is the area of the airfoil, Z_u and Z_l is the upper and lower height, taken from the x-axis, of the airfoil respectively and $\bar{z}$ is the neutral axis of the airfoil. The neutral axis of the airfoil is the camber line.

The blades are designed with a maximum value of stress that must be able to withstand, which in turn gives a required w for the airfoil since the moments of the blades come from aerodynamic forces and can not be altered. If the airfoil does not have this w so called spar caps are put on the inside of the blade in order to strengthen it, which means added weight. The spar caps are rectangles that is put at the thickest part the airfoil to make them as effective as possible. Thus finding an airfoil with the best aerodynamic performance for a certain value of w could in the end save weight of the blades.

2.2.2 Power coefficient

For the aerodynamic optimization the power coefficient, C_P, is chosen as the optimization target. It is used as a measurement for how different wind turbines compares with regards to aerodynamic performance. The power coefficient is a ratio between the power extracted and the power available in the wind [8] and defined as

$$C_P = \frac{P}{1/2\rho S U_\infty^3}. \tag{2.6}$$

Here P is the power extracted, ρ is the density of the flow and S is the frontal surface of the turbine. C_P for 2D was calculated based on the actuator cylinder (AC) model developed by Madsen [10] and followed the model as presented in a paper by Cheng et al. [11] with some modifications. When comparing different models for VAWTs the AC model has been shown to give as accurate or better results [12].

2.2.2.1 The actuator cylinder model

The AC model gets it name from modelling the swept area of the turbine as a cylinder. It assumes that the cylinder is infinite in the z-direction which gives a

two dimensional flow. The flow is quasi-steady and viscous effects are not considered, meaning that the governing equations are the Euler and continuity equations. The model is built on the idea that the aerodynamic performance was obtained by solving two equations: calculate the blade forces that depend on the flow field and calculate the flow field when the blade forces are known [10]. The flow field influences the blade forces which in turn influences the flow field. The AC model can capture how the moving blades, solidity, azimuth and angle of attack influence the flow which makes it a good estimator of turbine performance. At least for VAWT with a solidity that is small enough, meaning the blades should not be of such a size that the flow does not properly recover before the next blade passes through it.

When the blade moves through the flow it slows it down, called induction, and the induced velocity v is how much the flow is slowed down due to the induction. This influences the local velocity at the blades and therefore by influencing the local flow field at the blade, influence the blade forces. In the AC model the forces resulting from the blade forces are applied as volume forces Q_n and Q_t in the tangential and normal direction to the rotational plane respectively. The non-dimensional loads are calculated analytically according to equation 2.7 where U_{rel} is the relative velocity at the blade.

$$\begin{aligned} Q_n &= \frac{\sigma}{2\pi} U_{rel}^2 (C_l \cos\alpha + C_d \sin\alpha) \\ Q_t &= -\frac{\sigma}{2\pi} U_{rel}^2 (C_l \sin\alpha - C_d \cos\alpha) \end{aligned} \tag{2.7}$$

The values of C_l and C_d used in the AC method are interpolated from pre-computed polars. The polars are used as a look-up table in the AC method to obtain C_l and C_d for an angle of attack that it has calculated but was not pre-computed. The flow at the blade is obtained by superposition of the free stream velocity U_∞, the induced velocity w and the rotational velocity and normalized with U_∞ according to equation 2.8 with its components in the x and y direction.

$$\begin{aligned} U_{rel,x} &= 1 + v_x + \lambda \cos\theta \\ U_{rel,y} &= v_y + \lambda \sin\theta \end{aligned} \tag{2.8}$$

where $U_{rel,x}$ and $U_{rel,y}$ are the relative velocities in x and y direction respectively and v_x and v_y are the induced velocities in x and y direction. Due to the fact that v_x and v_y depend on Q_n and Q_t, which in turn depend on v_x and v_y, these values need to iteratively be calculated until the blades are in equilibrium. They are calculated for the whole rotation at the same time since the downwind flow depend on how much energy was extracted by the blades in the upwind flow as well as the flow at angle θ_i is affected by the flow at its neighbouring angles and flow at θ further away affects it less.

To save computing time the velocity is simply modified by a factor based on the relationship between induction and thrust coefficient, C_T and which has been empirically been determined by comparing with experimental data [11]. C_T is defined as

$$C_T = \frac{T}{\frac{1}{2}\rho S U_\infty^2}, \tag{2.9}$$

where T is the thrust, ρ is the density of the flow and S is the frontal surface of the blades [8].

C_P is then obtained as

$$C_P = -\lambda \sum_{i=1}^{n} Q_t d\theta \tag{2.10}$$

where the azimuth for one full rotation has been discretized with Q_t calculated for each azimuth step and finally summarized to get for one full rotation of the wind turbine.

A modification from the paper by Cheng et al. [11] is calculating the induced velocity for every blade at every time step instead of pre-computing it and use the same for every run. This should give a more accurate C_P since the shape of each airfoil is taken into account when obtaining the induced velocity.

2.3 Parameterization

To be able to optimize an airfoil, or any shape, it must be described by a finite number of variables which is done with parameterization. There exists many different parameterization techniques for obtaining an airfoil. According to a previous study by Giannakoglou [13] the parameterization of an airfoil should fulfill:

1. not limit the search space and also obtain "non-traditional" shapes
2. as few design parameters as possible
3. junctions of curves should not have discontinuities
4. negligible design variables should be excluded to not delay the convergence due to a noise in the fitness function
5. have design variables that are connected to the constraints

Of the various parameterization techniques, Bézier curves have been chosen since they fulfill all but the last conditions for a good parameterization [13].

A Bézier curve is defined as

$$\mathbf{B}(t) = \sum_{i=0}^{n} b_{i,n}(t)\mathbf{P}_i = \sum_{i=0}^{n} \binom{n}{i} (1-t)^{n-i} t^i \mathbf{P}_i \tag{2.11}$$

where $b_{i,n}(t)$ are the so called Bernstein polynomials, $\mathbf{P}_i$ is the Bézier points that define the curve, n is the order of the curve, $i = n+1$ is the number of Bézier points and $0 \leq t \leq 1$. The curve is controlled by the Bézier points and passes through the first and last one, but not necessarily any Bézier points in between, as can be seen in figure 2.6. Simplified, the curve can be imagined to be pulled towards the points that is between the end points.

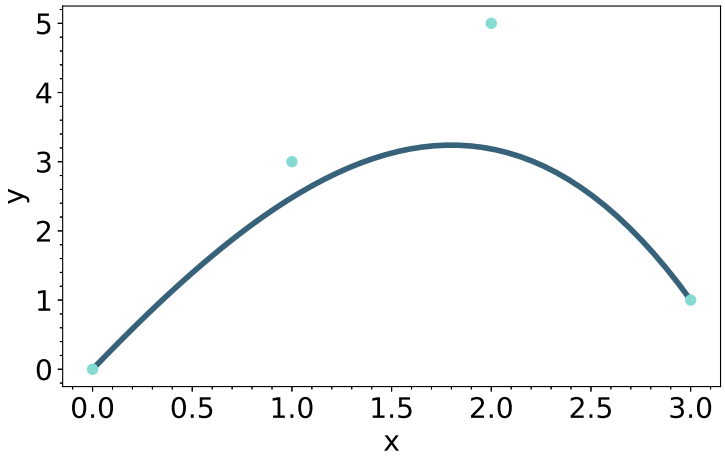

Figure 2.6: An example of a Bézier curve in blue with four Bézier points shown in a lighter blue.

The airfoils are expected to have the leading edge at $x/c = 0$ and trailing edge at $x/c = 1$ which is easy to implement using Bézier curves. A drawback is that changing the position of one Bézier point influences the whole shape of the curve and localized changes could therefore be difficult to obtain [13].

2.4 Optimization

In short, optimization is the selection of a value that best fit a certain criteria from a set of values. The function $f(x)$ that is to be optimized is called the objective function and the variables x are called decision variables. Optimization is usually based around minimizing a function, or multiple functions for multi-objective optimization, but it is also possible to maximize a function since $\max f(x) = \min 1/f(x)$. Thus, writing that the goal is to maximize the objective functions and describing the algorithms in terms of minimizing can be thought of as interchangeable. Optimization can also be set with or without constraints depending on the problem.

For constrained optimization the variables must satisfy a certain criteria. Constraints can both be required conditions for the variables or a penalty to the objective function for a certain set of variables. Without constraints the algorithm only optimizes after the objective functions with no regard to whether or not the resulting Bézier points gives a desirable shape for the end goal of this thesis. There are many different choices for type of optimization algorithms and two of them are: genetic algorithms and gradient based algorithms.

The optimization is considered constrained multi-objective. The two objective functions are maximizing w and maximizing C_P. There is constraints set on the decision variables to ensure an airfoil shape is obtained. Note that the objectives are conflicting, with maximizing w aiming for a thick airfoil while maximizing C_P aims for a thinner airfoil.

2.4.1 Pareto solution

For multi-objective optimization problems there is, usually, not a single optimal solution (airfoil) but instead a set of optimal solutions which fulfills the two objectives to a varying degree. The solution is considered optimal if at least one of the objective values are better and the other is not worse compared to another solution, then this optimal solution is called non-dominated [14]. The non-dominated solutions are also called Pareto-solutions which are considered to be along the Pareto front in figure 2.7. In other words, the Pareto front consist of the best solutions with regard to the objective functions with varying degree of compromise between the two and thus it visualizes the trade-off between the objective functions of the optimal solutions.

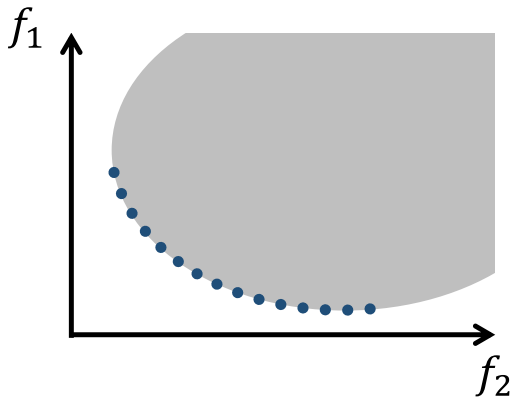

Figure 2.7: Pareto front in blue of all possible solutions in the objective space in grey when minimizing the two objective functions f_1 and f_2.

2.4.2 Genetic algorithm

The optimization is done using a genetic algorithm (GA) since it can evaluate a large amount of different candidates and has been used in similar studies by Giannakoglou [13] as well as Ferreira and Guerts [5] with good results previously. GAs are stochastic algorithms developed with inspiration from evolution and the mechanics of natural selection with a population of individuals that carry over their genes to the next generation. Due to the stochastic nature of a GA the final solution found might be a local optima, which might be different for different runs of the algorithm, and not the global [15]. As with evolution and natural selection the individuals that have the best genes with regards to some criteria are the ones who are passed on to the next generation with the best genes surviving for multiple generations. This is implemented with operators that are called survival, selection, cross-over and mutation with the genes described by decision variables.

In a GA a initial population consisting of N individuals is first created which can be either randomly generated or consist of individuals in an initial data set. The individuals in a generation are described by a number of variables n which are called genes in a GA since that is used as their biological counterpart. Every individual is evaluated in terms of how well it fulfills the objective functions and the different

operations are carried out in the order shown in figure 2.8. A central part is determining which individuals best fulfill the objective functions, how well they fit the problem at hand, and how to keep those features in the next population.

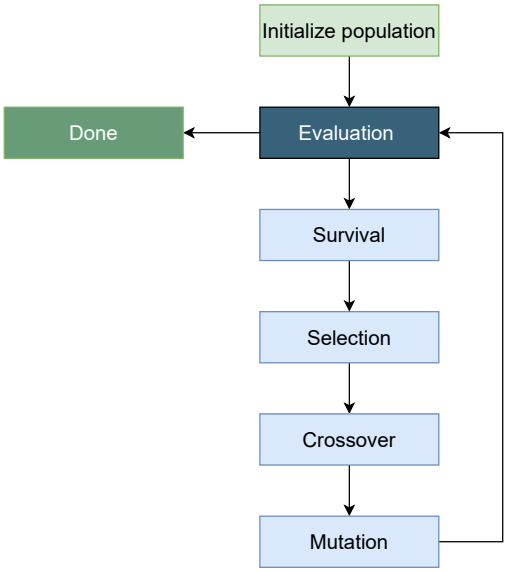

Figure 2.8: The basic steps of the GA with the operations shown as blue boxes. The algorithm is considered done when the stopping criteria is reached.

To reach the end goal of finding the optimal solution the best individuals in terms of fulfilling the objective functions should be carried over to the next generation. These operations in combination determine this and in short they do:

Survival Determining which individuals are best suited to survive to the next generation. Each individual gets a fitness value that is calculated from the fitness functions, usually the objective functions or some alteration of it. The individuals are ordered in terms of fitness.

Selection Select the individuals that are going to pass on their genes. Based on the fitness value with a higher fitness value giving a higher chance of being chosen. Depending on the choice of selection a certain number of individuals are chosen as possible parents.

Cross-over With probability p_c the cross-over between two individuals takes place and creates two new individuals that are a combination of the first individuals [16].

Mutation With probability p_m an individual gets a random change to one parameter. A rule of thumb is to set $p_m = 1/n$. Then on average one gene of an individual is mutated each generation. Helps with diversity in the population.

Another important concept is elitism. Since individuals are chosen based on probability the individuals with the highest fitness value is not guaranteed to be chosen for mating and thus valuable candidates for an optimal solution is lost. To mitigate this the individuals with the highest fitness value is copied to the next generation regardless [15].

2.4.2.1 Chosen algorithm: NSGA-II

The algorithm chosen is non-dominated sorting genetic algorithm 2 (NSGA-II) which is implemented with the `pymoo` [16] library in Python. NSGA-II is developed with multi-objective optimization in mind and has been shown to have diverse optimal solutions, lower computational complexity and converges close to the Pareto optimal set. This comes from the algorithm using fast non-dominated sorting, crowding distance together with crowding comparison and utilizing elitism.

Fast non-dominated sorting sorts the individuals of the population into non-dominated solutions and dominated solutions. It assigns the non-dominated solutions to the first front $\mathcal{F}_1$. Then the dominated front is sorted into non-dominated solutions and dominated solutions with the non-dominated solutions assigned to front $\mathcal{F}_2$, this is continued until the population is sorted into $\mathcal{F}_k$ number of fronts. Its preserving diversity by using crowding distance. The density of the solutions is estimated by checking the distance between different solutions in the objective function space. Then a crowding comparison is carried out that assigns a crowding distance value depending on how far one solution is to another solution.

NSGA-II creates the next population P_{i+1} by combining the current population P_i with the previous population P_{i-1} into a combined population of size $2N$. The $2N$ individuals are sorted into fronts with fast non-dominated sorting as shown in figure 2.9. This ensures elitism since the previous best solutions is carried over to the next generation. To obtain an offspring population the front $\mathcal{F}_1$ and the subsequent fronts based on fitness up to front $\mathcal{F}_l$ are chosen. The individuals up to front $\mathcal{F}_l$ are most likely not exactly N therefore the last front $\mathcal{F}_l$ is sorted by crowding comparison and individuals are added to the next population in descending order until all populations slots are filled. With crowding distance binary tournament selection is built into the algorithm with selection based on both elitism and crowding distance. P_{t+1} is then created with selection, cross-over and mutation where selection is a binary tournament selection with the crowding comparison as the selection operator [14].

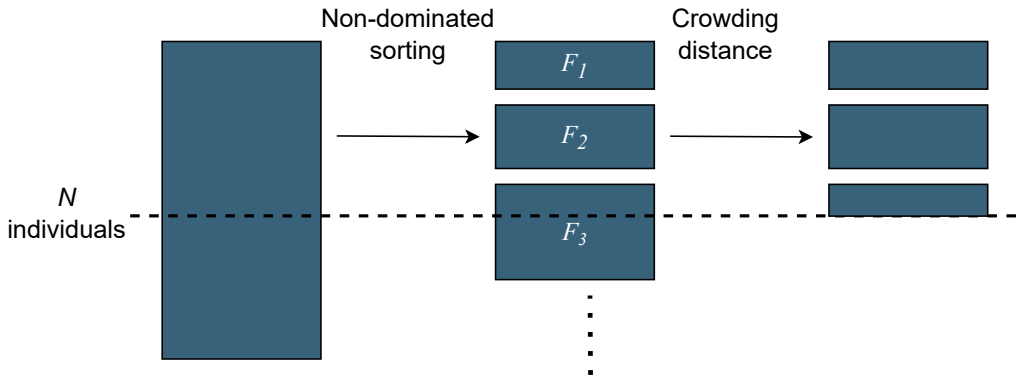

Figure 2.9: Simplified view of the NSGA-II procedure. Crowding distance is used on front $\mathcal{F}_3$ to keep N individuals for the next generation. Adapted from [14].

2.4.2.2 Parallelization

A large advantage with genetic algorithms is that it is possible to run the fitness evaluations of the individuals of one generation in parallel and thus save computing time. The evaluation of one individual has no influence on the other individuals in the generation and the connection between individuals only comes into play when selection and cross-over should be performed. The pymoo library also comes with a parallelization function which uses the so called `starmap` object which allows multiple arguments to be sent to the parallel function, ie the evaluate function. The number of parallel executions need to be specified and should utilize as many cores as possible.

2.5 XFoil

XFoil is a software developed for design and analysis of airfoils at subsonic flows and is based on a panel method [17]. Panel methods are a numerical method used to solve the flow equations for potential flow (inviscid and irrotational flow) over a surface that is divided into discrete panels which makes the calculations quick. XFoil was developed with the goal to combine the high speed and accuracy of higher order panel methods with a fully coupled inviscid/viscous interaction method that was already developed. It has various useful functions regarding airfoils built in [17].

XFoil automatically handles the special way airfoil data is stored, i.e. counter clockwise from top trailing edge to bottom trailing edge. This makes it a very useful and easy to use tool when working with airfoils. Though it is very important that the airfoil goes through true zero otherwise XFoil has difficulties due to the shape not being what is expected of an airfoil profile. XFoil can among other things calculate polar for an airfoil over a given range of angle of attacks but since the flow is very simplified the accuracy of the results sometimes suffers. Lift is usually over-estimated while drag is under-estimated [18].

It is however deemed that the accuracy lost in the polar curves is more than compensated for with how much quicker XFoil can obtain them compared to CFD. When also considering the limited computing power available XFOIL is very useful when at a first design stage in order to be able to investigate a large number of diverse airfoils. However, XFoil is sensitive to the shape that it calculates the flow over. If it is not similar to an airfoil then XFoil might have trouble converging or it can obtain unreasonable results. It also struggles if the shape is rough and of poor quality with the leading and trailing edge being the most sensitive areas regarding this. It is however very quick to obtain the polars with XFoil which makes it a good fit for designing VAWT airfoil profiles [5], [13], [19]–[22]. In summary, XFoil can calculate the polars which in combination with the actuator cylinder method evaluate the C_P for a large number of airfoils with limited computing costs.

3
Methods

To achieve the goal of obtaining a family of optimized airfoils an optimization method is implemented. Since the airfoils is optimized with regards to both the power coefficient and the section modulus a dual-objective algorithm were used.

In Python a bi-objective GA were set up with the two objective functions of maximizing section modulus and maximizing the power coefficient. The variables of the GA are the x and y coordinates of the Bézier points that describe the airfoil. Therefore the airfoils must be parameterized in order to feed them to the algorithm and in turn obtain new optimized airfoil shapes. The section modulus is calculated directly in Python and the power coefficient is obtained with the actuator cylinder method based on the airfoil polar obtained from XFoil.

3.1 Parameterization

Part of the initial generation of the GA are made up of known airfoils, see appendix A.1 for a complete list. These must be parameterized as Bézier curves in order to obtain the variables, x- and y-coordinates of the Bézier points, for the algorithm. Since, as stated previously in section 2.3, a Bézier curve starts and stops at the first respectively the last point the top and bottom half of the airfoil are parameterized independently to ensure that the leading and trailing edge are located $x/c = 0$ and $x/c = 1$ respectively. After the independent curves are created they were simply put together and treated as a complete airfoil with the data points sorted in the typical airfoil ordering.

3.1.1 Refinement of known airfoils

Before parameterization of the known airfoils some of them had to be refined due to them having quite few data points which resulted in an airfoil shape that were very rough to the degree that especially the leading edge had sharp edges. The airfoil data was refined by using XFoil's re-paneling method which by interpolating can create more panels along the airfoil. By re-paneling with a higher amount of panels the number of data points describing the shape of the airfoil is also increased. It is paramount that the airfoils given to XFoil are of a good quality, especially having a good leading edge, otherwise the polar curves can be badly estimated due to the airfoil being rough. In figure 3.1 the leading edge for one of the airfoils is clearly smoother after refinement and thus XFoil can more accurately calculate the

aerodynamic properties of the airfoil.

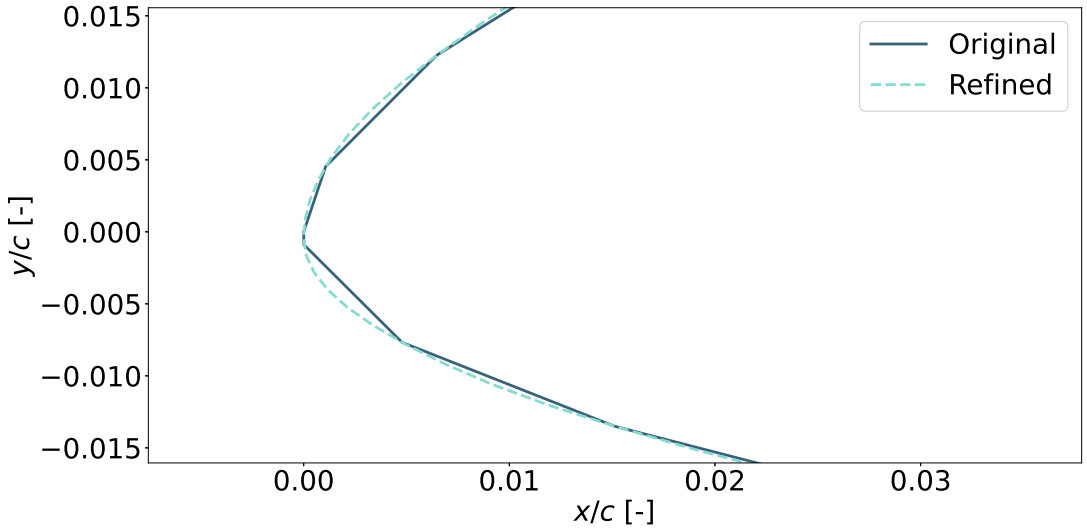

Figure 3.1: Refinement of the DF 101 airfoil at the leading edge.

Unfortunately the refinement yields that the leading edge might not be located at $x/c, y/c = (0, 0)$ due to how XFoil re-panels the airfoil. Due to this the refinement was only done for the airfoils with too few data points to not risk obtaining more inaccurate polars. For the badly refined airfoils the gain in accuracy with a smoother leading edge compensated for the risk of worse polars with a leading edge located at a different point than $x/c, y/c = (0, 0)$.

3.1.2 Bézier points from known airfoils

The Bézier points were obtained by using a least square fit function which aimed to minimize the difference between the known airfoil and the Bézier curve with the x and y coordinates of the original airfoil and the Bézier curve according to

$$\min f = \min \sum \sqrt{(x_i^{\text{original}} - x_i^{\text{Bézier}})^2 + (y_i^{\text{original}} - y_i^{\text{Bézier}})^2} \tag{3.1}$$

To limit the search space and ensure a desirable shape the bounds and constraints in table 3.1 were implemented. The bounds and constraints were similar to the ones that would later be implemented in the optimization algorithm to ensure that the first generation would fulfill these. The bounds are from the normalization of the airfoil length and thickness in order to limit the search space and constraints are in part from how XFoil expects airfoil data to be. Constraints of the Bézier points neighbouring the leading edge points was set in order to ensure that the sensitive trailing edge were a smooth curve since the minimization would sometimes not achieve this otherwise.

Table 3.1: Bounds and constraints set for obtaining parameterized airfoils.

Bounds		
$0 \leq x \leq 1$ $-1 \leq y \leq 1$		
Constraints		
Bézier point location	Value	
Leading edge	$x = 0$	$y = 0$
Leading edge top neighbour	$x = 0$	$0 < y < 1$
Leading edge bot neighbour	$x = 0$	$-1 < y < 0$
Trailing edge	$x = 1$	$0 < y < 0.005$

3.1.2.1 Number of Bézier points

A convergence study was conducted to find how many points were required to obtain a good fit between the original airfoil and the Bézier curve. The number of Bézier points influences the shape of the curve with a higher number of points ensuring that more complex shapes are possible to create. However, more Bézier points also means that changing the position of one Bézier point has less influence of the over all shape. Thus a greater shape variation requires a changed position of more Bézier points. Therefore the number of Bézier points should be somewhat limited. Note that the heaviest part computationally is obtaining the aerodynamic values from XFoil regardless of number of Bézier points since it is the Bézier curve that is sent to XFoil.

The convergence study utilized XFoil and thus the result should not be influenced by a bad airfoil shape. Therefore an airfoil from the NACA 00xx-series was chosen since they can be created analytically which gives them a high resolution for the entire chord. The NACA 0018 was chosen since it is often used in VAWT. The study was done by calculating the relative error, δe, of C_l at an angle of attack of 2 and C_d at an angle of attack of 0 according to

$$\delta e = \frac{C^{\text{Bézier}} - C^{\text{original}}}{C^{\text{original}}}, \tag{3.2}$$

where C is either of the coefficients. The polars were obtained from XFoil for both the original airfoil and the Bézier curve.

The function value from equation 3.1 in figure 3.2 decreased with an increasing number of Bézier points which means that a higher number of Bézier points give a closer fit of the airfoil. However, the error of the function value does not consider whether or not the difference between the Bézier curve and the known airfoil is at a place where a small geometric change results in large differences in aerodynamic properties therefore it should not be the only deciding factor for the number of Bézier points.

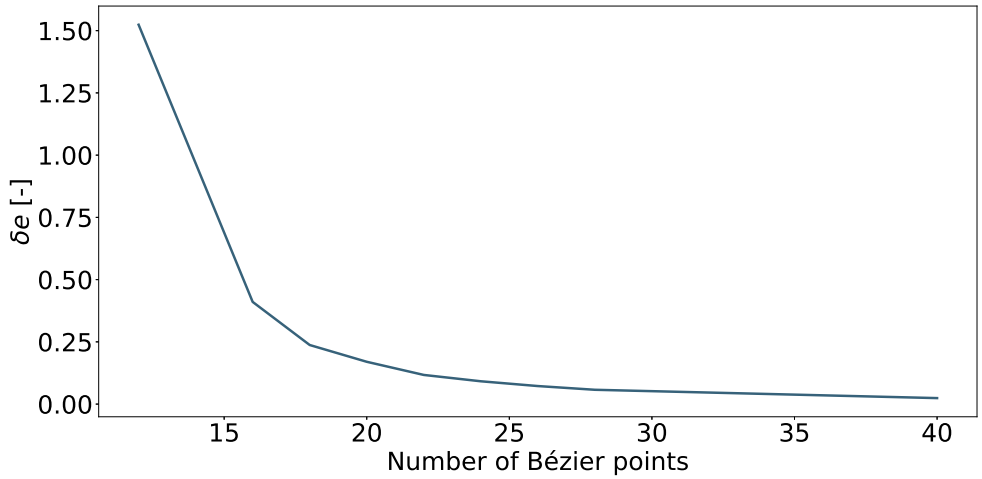

Figure 3.2: The function value of equation 3.2 for an increasing number of Bézier points.

The error of C_d and C_l in figure 3.3 does not have one clear value of Bézier points that would be best. For the error of C_d in figure 3.3a any number of Bézier points apart from 20 is more or less equally good whereas where as the error of C_l in figure 3.3b it oscillates slightly around zero for all Bézier points with 22 and 26 points giving the highest absolute error. Taking this into consideration 24 Bézier points were chosen since the error both in figure 3.2 and in figure 3.3 are considered satisfyingly low.

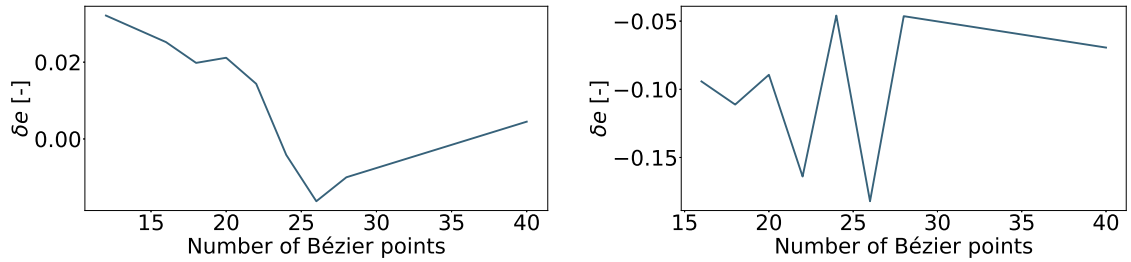

(a) Error of C_d **(b)** Error of C_l

Figure 3.3: The error at an angle of attack of zero degrees for an increasing number of Bézier points.

As a final check, the leading and trailing edge of a Bézier curve with 24 Bézier points were visually studied to ensure that it was as desired. That the leading and trailing edge of the airfoil is of good quality is of outmost importance to ensure that the polars from XFoil are accurate. With 24 Bézier points the leading edge and trailing edge of the fitted Bézier curve in figure 3.4 are smooth and well defined as well as following the known airfoil closely. The parameterization is therefore deemed to be of good enough quality and the number of Bézier points were set to 24 for the optimization.

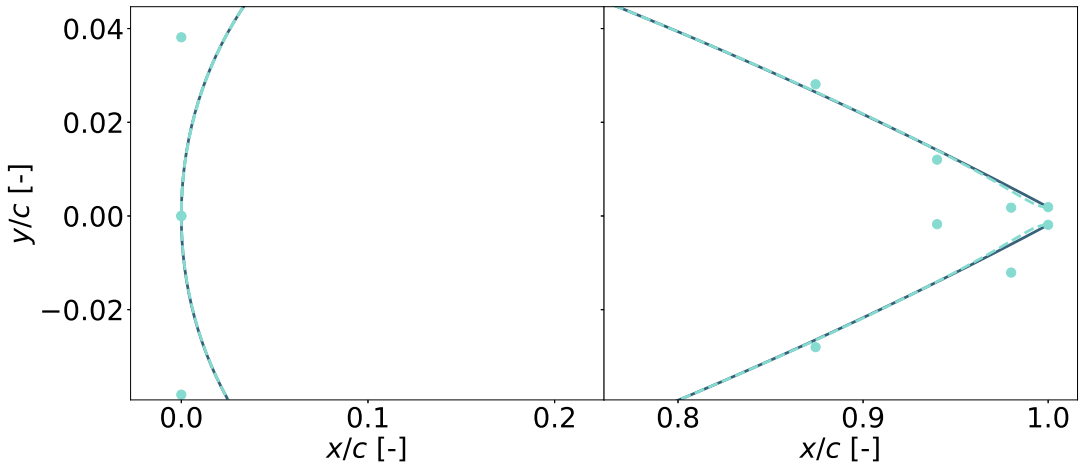

Figure 3.4: Leading and trailing edge of the NACA 0018 with a parameterization of 24 Bézier points. Unfortunately the trailing edge is not followed as close as the leading edge.

3.2 Optimization

To obtain the initial family of optimized airfoil a GA with the algorithm NSGA-II was set up using the Python library `pymoo`. The structural objective function were calculated directly in Python but for the aerodynamic objective function XFoil were utilized. `Pymoo` requires a certain set up of the constraints of the optimization and the parameters of the GA. XFoil can quickly calculate polars for an airfoil but due to the complexity in setting up the algorithm and obtaining C_P an optimization with a simpler aerodynamic objective function is first done as a way to ensure that the set-up of NSGA-II works as intended. Then the blade profile optimization were run to obtain the optimized family of airfoils.

3.2.1 Set up of NSGA-II

As mentioned previously, the x- and y-coordinates of the Bézier points are the decision variables for the GA. Some Bézier points are at the same position for every individual in every generation, e.g. the Bézier point at the trailing edge, and is therefore not considered a decision variable. This avoids any mutation that would later be nullified by constraints. The decision variables are in a vector with the same ordered from top trailing edge to bot trailing edge passing the leading edge. The constant Bézier points are added to this vector before obtaining the Bézier curve and then the fitness values is calculated. The GAs initial population consists of a mix of already existing airfoils, airfoils obtained from a previous optimization study by Ferreira and Guerts [5] as well as randomly generated airfoil profiles. Thus giving the algorithm a diverse range of shapes as a starting point with airfoils that already has good aerodynamic and structural properties, though not good enough for the aim of this thesis, as well as a randomness that helps with finding new airfoils.

3.2.1.1 Constraints

Constraints were set up to ensure that airfoils were obtained and not arbitrary shapes that fulfilled the objective functions. Bounds on the search space is also set to limit the algorithm setting variables that results in non-airfoil shapes.

As stated previously, an airfoil is usually represented with normalized coordinates in both x and y direction with a chord length of 1, which gives a clear limit for the search space for the x-coordinate variables. That the airfoil might be cambered must be considered when setting the bounds for the y coordinates. While an airfoil with a thickness that goes to $y/c = \pm 1$ is not reasonable, the bounds are for the y-coordinates of the Bézier points and could be a reasonable value for a single Bézier point.

The trailing edge should have a height and not be pointy while also not be too thick, therefore constraints were set. The thickness over the trailing edge were set to be around the x-axis in order to ensure that the chord would still be 1, otherwise different sizes of airfoils would be compared. The limits for the thickness was obtained from the first generation of airfoils. The trailing edge max thickness is simply the thickest of any airfoil and the min value was taken from the NACA 0006 since it is a very thin but still a manufacturable airfoil. This gives bounds and constraints according to table 3.2.

Table 3.2: Bounds and constraints set in the optimization algorithm.

Bounds	Constraints	
$0 \leq x \leq 1$	Where	Value
$-1 \leq y \leq 1$	Trailing edge Bézier point	$0.0006 < y < 0.01$

3.2.1.2 Aerodynamic parameters

To best capture the conditions the wind turbine operates in the parameters in XFoil were set according to table 3.3. While it may seem redundant with both specifying a dirty blade and setting a trip wire for earlier detachment of the boundary layer it is set in that was in case the boundary layer would starting detaching earlier than the trip location due to the dirty condition for some airfoil.

Table 3.3: Parameters set up for polar and C_P calculations. Dirty influences the transition from a laminar to a turbulent boundary layer.

Condition of blade	Dirty
Boundary layer trip wire location	0.05
Re	$1 \cdot 10^6$
α	[0, 2]

3.2.2 Strut optimization

As a stepping stone and a way to validate that the optimization algorithm works as intended, the profile of the struts of the VAWT was the target for optimization. The struts are symmetrical and the aerodynamic objective function minimize C_d is easier to implement and takes less computing time than calculating C_p, due to the AC method requiring a wider range of angle of attacks and internal iterations. The minimization of C_d was set to be the average value over the range of $0 \leq \alpha \leq 2$ to ensure a non-specialized shape.

For this step parallelization the built in `StarmapParallelisation` function was used in pymoo was implemented. This enabled evaluation of airfoils within the same generation to be evaluated in parallel on the different cores on the computer which saved a lot of computing time.

Some of the obtained Pareto front airfoils had un-airfoil like shapes as in figure 3.5, i.e. very flat backs making the shape more similar to a bullet than an airfoil. XFoil still considered them to have an average C_d below 0.1 hence why they were able to survive to the next generation. The low and unrealistic C_d is due to XFoil not calculating the base drag, i.e. drag due to the low pressure region at the back of the airfoil. Somewhere during the optimization the airfoil shape is such that XFoil fails to properly evaluate the drag coefficient and drastically underestimates it.

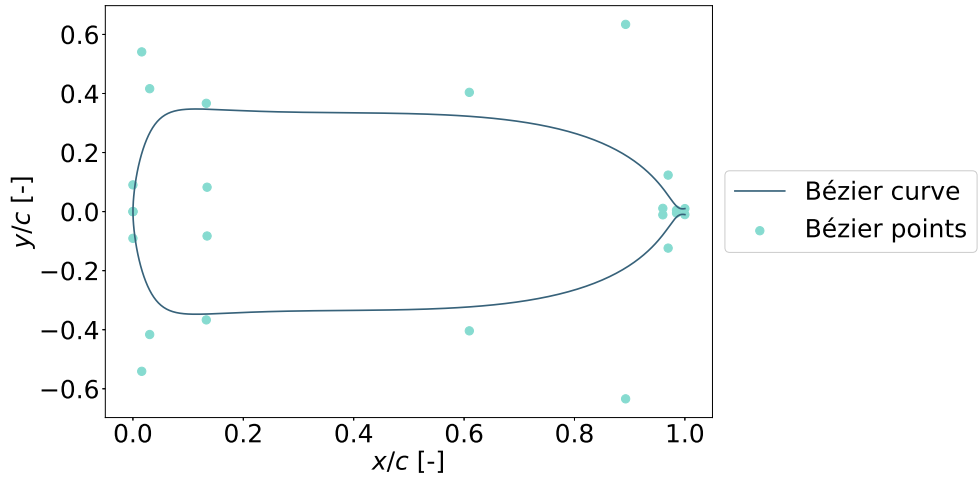

Figure 3.5: One of the Pareto-optimal individuals obtained from an optimization run without penalties implemented with an underestimated drag coefficient.

Hence, somehow limiting the algorithm to avoid obtaining the shapes for which XFoil is unable to properly evaluate the lift and drag were needed. Further constraints on the Bézier points could be difficult to implement and instead penalties were added to the fitness function values when an unwanted airfoil shape was generated.

3.2.2.1 Penalties on the geometry

Penalties were added to airfoils which obtained an obviously unwanted airfoil shape. The penalties were to help the algorithm with excluding undesired shapes that XFoil did not properly calculate the polars for. The penalties were added making sure to not limit the creativity of the airfoil and discard a good shape. All penalties were based on the geometry of the airfoil and gave the benefit of discarding airfoils before the polars were calculated and thus save computing time. Three different functions were added to check whether an airfoil should get a penalty or not.

To further limit unwanted shapes a bound on the Bézier curve was added. The bound in figure 3.6 was based on the maximum y-value with a factor of 1.1 added at every x-coordinate of the initial population. Since the initial population also has airfoils that are considered very thick, too thick for a wind turbine even, this constraint is not considered too harsh. To avoid obtaining airfoils for which XFoil is not able to properly evaluate the lift and drag coefficients the bound at the leading and trailing edge was slightly altered. The leading edge got a gradually increasing factor to ensure a non-flat front and the trailing edge was set according to their upper constraints in table 3.2 since a trailing edge outside this would still be discarded. This keeps the creativity of the GA within reasonable bounds when XFoil does not capture that an unreasonable shape has been created.

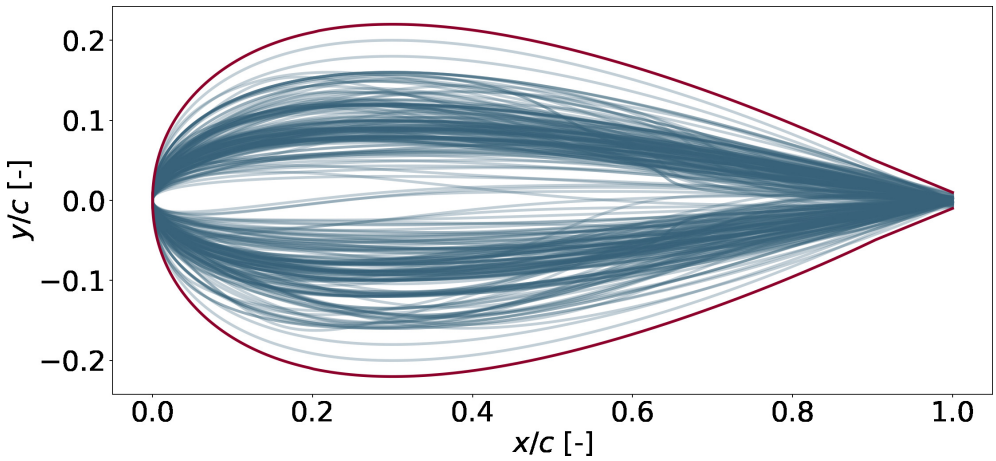

Figure 3.6: Bounds that limit the y-coordinate of the airfoil

To avoid a flat back of the airfoil a limit on the curvature of the Bézier curve was added. The curvature, κ, for a parameterized curve $\gamma = x(t), y(t)$ is calculated according to

$$\kappa = \frac{|x'y'' - y'x''|}{(x'^2 + y'^2)^{3/2}} \tag{3.3}$$

where the derivatives have been taken with regard to t. It gives the curvature for each point along the Bézier curve. The curvature was calculated for the initial pop-

ulation to get a reasonable limiting value of κ. Due to the overall shape of an airfoil with the thickest part of the airfoil usually located towards the leading edge, there is two different threshold values for κ.

To avoid obtaining overly thick airfoils the maximum thickness of the airfoils were limited. The thickness was taken as the maximum difference between the upper and lower half of the Bézier curve. While the Bézier curve is described by a lot of discretized data points it is still discretized and thus the thickness is not the exact analytical value. Therefore the maximum allowable thickness was set to $t/c = 41\%$.

3.2.2.2 Set up of strut optimization

The algorithm for the evaluation of an airfoil was, in a simplified view, set up as in figure 3.7. With the added penalty check for the geometry before calling XFoil computing time was saved. The evaluation and following steps until the fitness values were obtained were done in parallel for the airfoils in a generation. With this set-up struts that were deemed to be of reasonable shape was obtained and the blade optimization was started with the strut optimization set-up as a starting point.

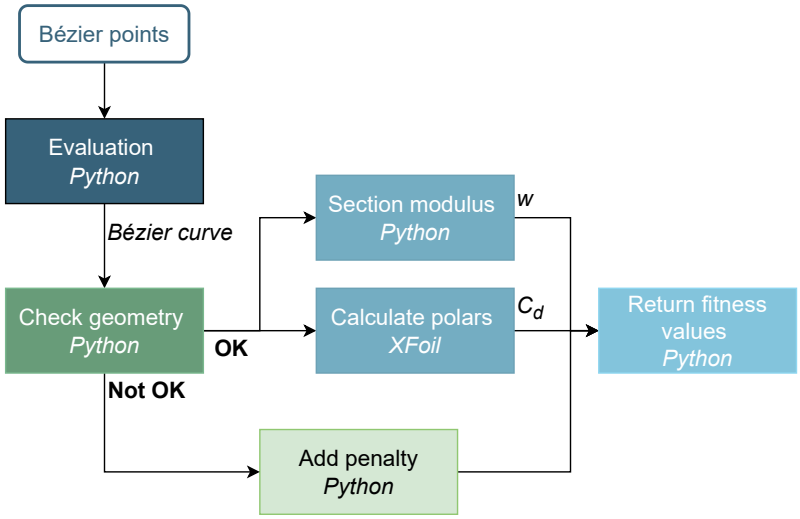

Figure 3.7: Simplified flow chart of the evaluation function for optimization of the struts with the functions and penalties check shown as boxes. The output from some functions are written out and is the input to the following function.

3.2.2.3 Convergence study

While the polar calculations with XFoil are relatively quick they still take a few hours due to the large number of polars that need to be evaluated. In order to not waste limited computing power a short study was conducted to determine what the parameters of the GA should be set to. The parameters in question are: population size, number of generations, crossover probability and mutation probability. The study was done with the set up for the strut optimization in section 3.2.2 since the

struts require fewer angle of attacks to be evaluated and thus the convergence study takes less computing time.

First the number of generations were checked by running the simulation for 500 generations and checking the average fitness value obtained each generation for the two fitness functions. The population size was set to 100 similarly to a previous study by Ferreira and Guerts [5] as a starting point. The fitness value for the two functions were averaged separately and gave an indication of when the population is starting to converge. After 200 generations in figure 3.8 both fitness values changes less for the coming generations. While it does still change, and interestingly the section modulus does somewhat become smaller for generations after 350, the computing time in figure 3.9 increases for each number of generations and thus 200 generations are deemed as a good fit.

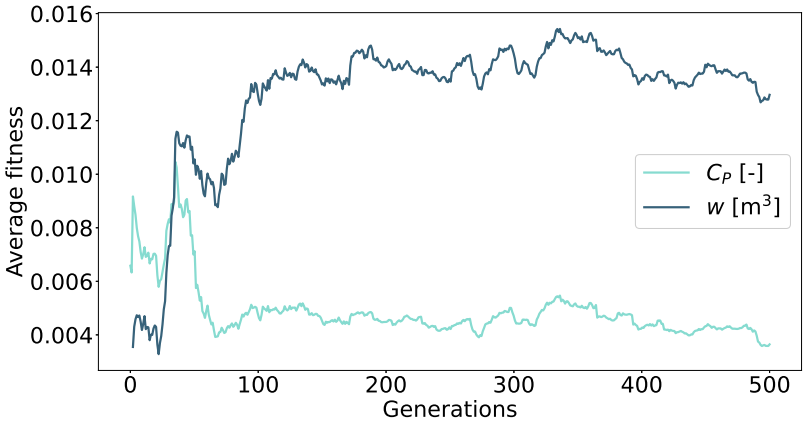

Figure 3.8: Average fitness value of each population consisting of 100 individuals for 500 generations.

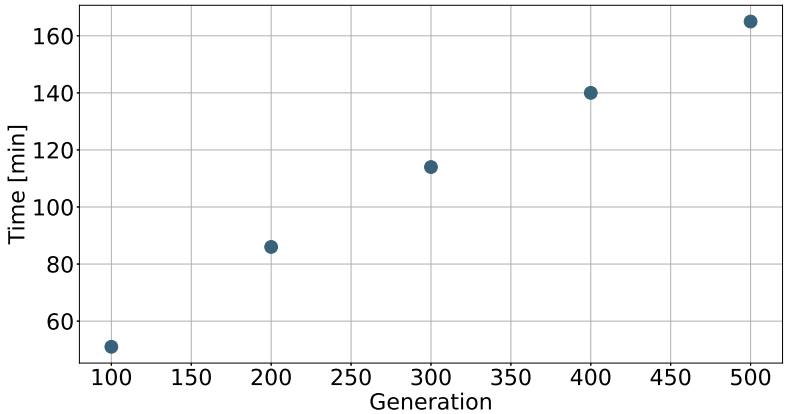

Figure 3.9: The total time for the full optimization with varying number of generations.

Then the size of the population was determined by comparing the Pareto front in terms of spread. Since the goal is to find a family of optimal airfoils it is of greater interest to obtain a wider spread of airfoils and a good amount of airfoils. The simulations were run for 200 generations with varying population size between 100 and 500 individuals.

For the four different population sizes in figure 3.10 a population size of 200 in figure 3.10b and a population size of 300 in figure 3.10c gives a wider front compared to a population size of 100 in figure 3.10a and a populations size of 500 in figure 3.10d. The number of individuals in front are about the same for 200, 300 and 500 population sizes but is much lower for a population size of 100. While the spread in the front and the number of Pareto optimal individuals can vary if the algorithm is run again it at least gives an indication that there is not a clear pattern with regards to population size.

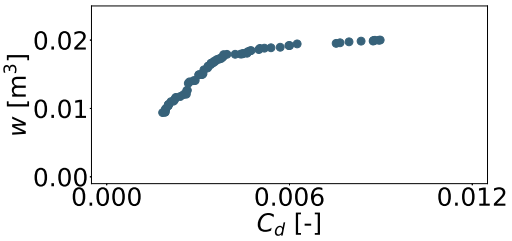

(a) Population size of 100 with 76 individuals in the front

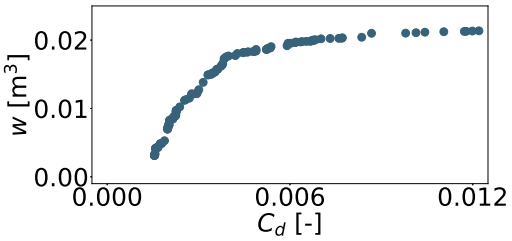

(b) Population size of 200 with 116 individuals in the front

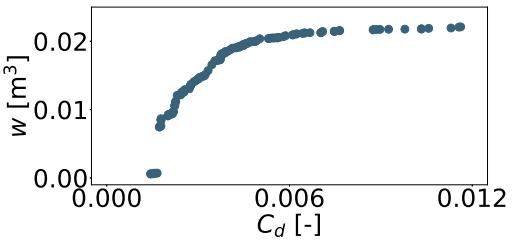

(c) Population size of 300 with 132 individuals in the front

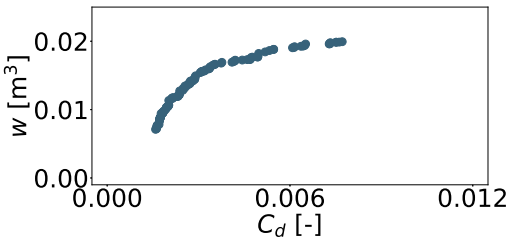

(d) Population size of 500 with 118 individuals in the front

Figure 3.10: The Pareto front for 4 different population sizes for the strut optimization algorithm.

With increasing population size the time it took to run a full optimization run in figure 3.11 increased with the growing population size. Considering the increase in time a population size of 200 is chosen since for the specific run it gave a more desirable result than 100 individuals but took short time to finish compared to a population size of 300.

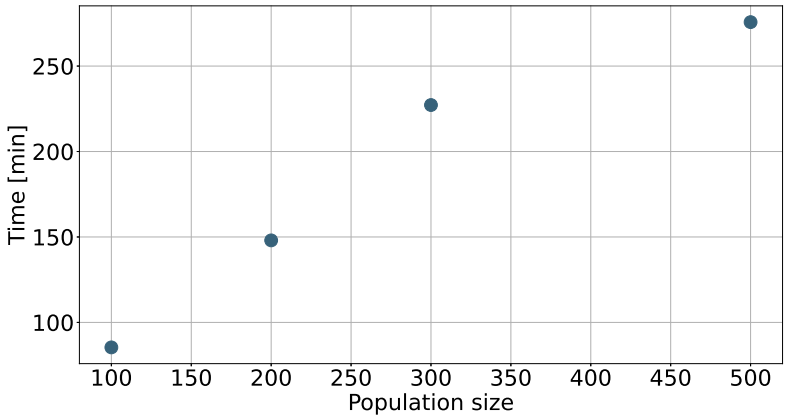

Figure 3.11: The time in minutes for an optimization with different population sizes

Due to time constraints no convergence study was done for the mutation and cross-over probability. The mutation probability was set to $p_m = 1/n$ based on the rule of thumb to achieve on average one mutation per individual [15]. The cross-over probability was set to $p_c = 0.95$ to ensure that cross-over was occurring often each generation.

3.2.3 Blade optimization

The blade optimization was done, as stated previously, with w as the structural optimization and C_P as the aerodynamic optimization. Calculating C_P was done with the AC method which required angle of attack, C_d and C_L that were still obtained with XFoil. This meant an additional step in the set up of the evaluation. The penalties that were added for the strut optimization were kept and continuing on the path of excluding airfoils before costly calculations penalty functions that checked the polars before the AC method was added.

3.2.3.1 Aerodynamic parameters for the AC method

The parameters related to XFoil was still set as earlier according to table 3.3 but some additional aerodynamic parameters in table 3.4 were required for the AC method. A new range of angles of attack was also required since the AC method uses calculated polars as a look up table in which it interpolates polars based on the obtained angle of attack.

Table 3.4: Parameters set up for C_P calculations.

α	$[-18°, 22°]$
λ	3
σ	0.15

3.2.3.2 Further penalties

The airfoil is no longer symmetrical which means that it is possible that the top and bottom Bézier curve intersects. This is of course not a reasonable candidate for an airfoil and thus one more geometrical constraint that checked if the curves intersected were added.

XFoil can sometimes fail to converge when calculating the polar for an angle of attack and return in invalid value, called a NaN. Since the AC method interpolates the angle of attack for different azimuth angles it was unwanted that the calculated polars contained too many NaN and risk an inaccurate interpolation. When stall occurs then the curve is no longer linear, see figure 2.3, and missing too many polars would then not capture the change in slope.

The AC method interpolates from the XFoil polars and calculates the angle of attack for every azimuth angle and could potentially obtain an angle of attack that was outside the polar range [11]. Then it is not certain if the angle of attack the AC method extrapolated was accurate. A penalty was therefore added if an angle of attack was extrapolated.

The AC method can also give unreasonable values on C_P and C_T. C_P is a ratio and should therefore only be a value between 0 and 1, if the value obtained was outside this range then a penalty was added. C_T is also a ratio but the theory does not follow empirical studies and can get values up to 2 but still not lower than 0 [8, p. 130]. Likewise if a value outside this range was obtained then a penalty was added.

3.2.3.3 Set up of blade optimization

After the penalties were added the set up of the simulation was according to figure 3.12. With the addition of the AC method the optimization requires further steps compared to the set up of the strut optimization in figure 3.7. The penalties were added at three different steps depending on the nature of the check but each was done as early as possible to discard airfoils without wasting computational time.

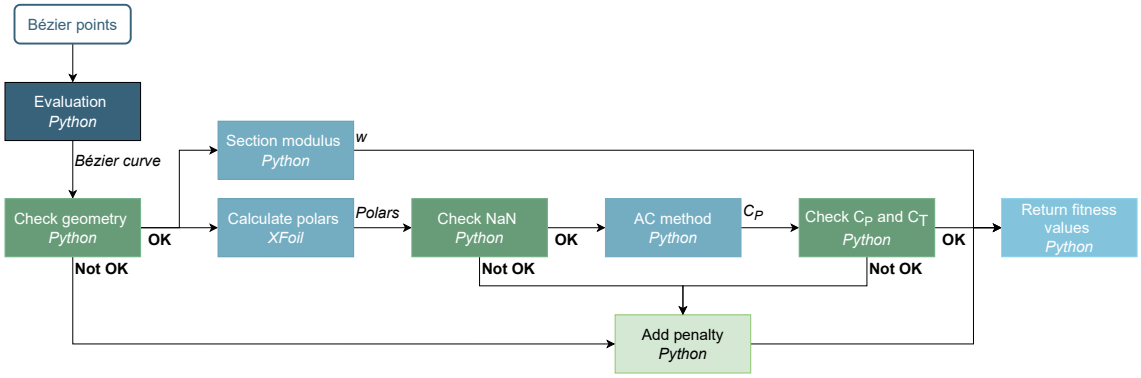

Figure 3.12: Simplified flow chart of the optimization algorithm for optimization of the blades with the functions and penalties check shown. The output from some function and the penalty checks are written out.

3.2.3.4 Check convergence

No new convergence study was made for the blade optimization. Instead the average power coefficient and section modulus in figure 3.13 were checked for the number of generations and population size that was obtained from the strut convergence study.

The change of w in figure 3.13a has a greater slope below 100 generations and then the slope gradually becomes flatter until it is flat after around 180 generations. While it is not long before 200 generations it is deemed that 200 generations is good also for the blade convergence. The C_P changes much more between generations but the slope after 100 generations goes steadily up until about 175 generations. Once again 200 generations is deemed a good fit also for the blade optimization.

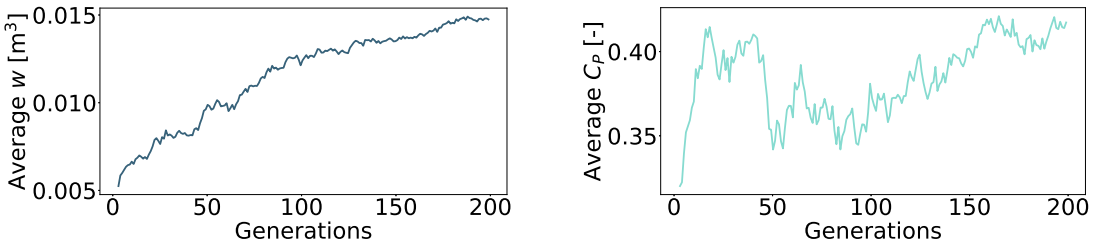

(a) Value of w **(b)** Value of C_P

Figure 3.13: Average fitness values for the objective functions of the blade optimization for 200 generations and a population size of 200.

4

Results

The obtained family of airfoil profiles for both the strut optimization and the blade optimization after simulations run with XFoil are presented and discussed. From the family of obtained blade profiles a few airfoils are further studied with regard to blade and turbine performance. The blade optimization was also done with a higher Reynolds number to see its impact on the design.

4.1 Strut optimization

From the set up explained in section 3.2.2 XFoil was called around 160 000 times (200 generations, 200 individuals and 4 angles of attack) and the run time was about 2,5 hours. This strongly shows the advantage of using XFoil despite its shortcomings with regards to estimating the polars.

The objective functions for the strut optimization were to maximize the section modulus and minimize the drag. The obtained fitness values for every evaluated individual in figure 4.1 has a trend of going towards the left as well as towards the top though this is not seen as clearly. For the first number of generations in light blue there is a larger spread between the individuals when the optimization has not yet found a shape to converge towards. For the last number of generations there is not as large a difference between individuals since the are covered by dark blue is smaller than the light blue. Implying that smaller improvements in terms of the fitness values were made for the later generations.

The obtained Pareto front is in dark blue and contains the non-dominated individuals for all generations. Though, the front is very straight covering only a small range of C_d but a large range of w. Such a small increase in C_d while still increasing w to that extent seems unreasonable. To the right of this front seems to be another front of individuals. What is more likely is that the front created by the rightmost set of individuals is the more reasonable optimized group of airfoils since it is for more reasonable values of C_d and not as small increase in w with decreasing C_d. This could be due to XFoil obtaining a shape that has drag that XFoil does not capture, such as base drag as discussed in section 3.2.2.

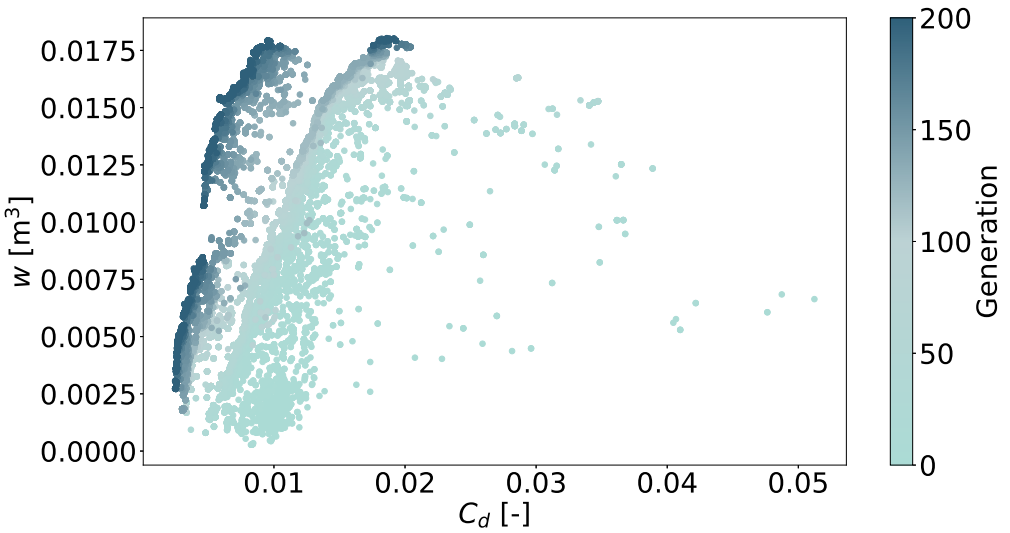

Figure 4.1: Every evaluated individual for one full strut optimization. The first generations are in a light blue color which gradually changes to a dark blue for the later generations.

The Pareto front contains individuals with very low C_d in figure 4.2. While the front is most likely not reasonable the individuals in the top right corner seems to have a reasonable C_d. The location and orientation of the front comes from that the objective functions is to minimize C_d and maximizing w. With the decreasing C_d the individuals seem to become more clumped together and especially the individuals furthest to the left have almost all the same C_d but different w which is not expected as there should be a trade off between the two objective functions. The obtained values of C_d for the majority in this front is also unreasonable low considering their values of w.

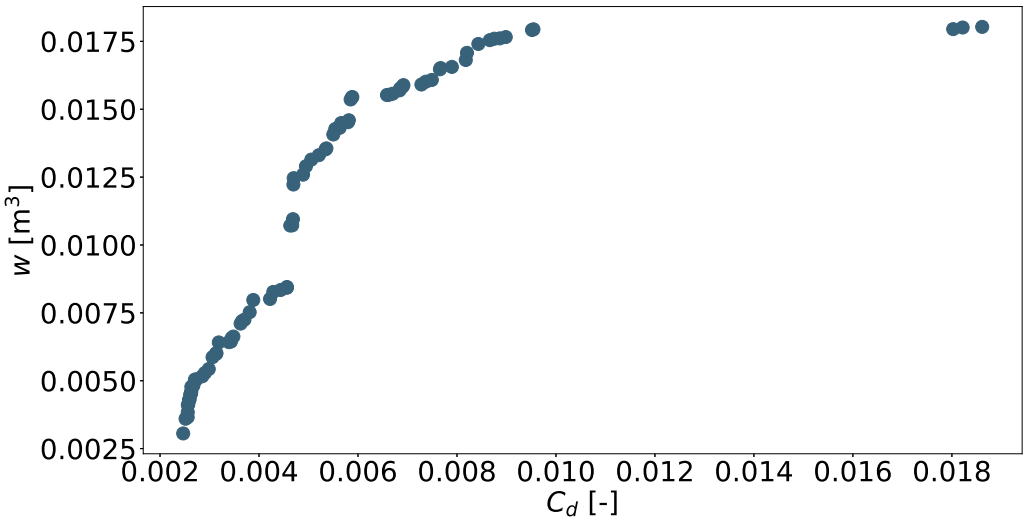

Figure 4.2: Pareto front with 91 individuals obtained from the strut optimization.

The obtained struts in the Pareto front in figure 4.3 shows a spread in thickness which matches with the spread in w in figure 4.2, though that there are many thick individuals does not match with the obtained values of C_d. Some of the thickest ones could have separation that XFoil does not capture and therefore greatly underestimates the drag. Some of the less thick ones could potentially be interesting for the struts and depending on their requirement for w.

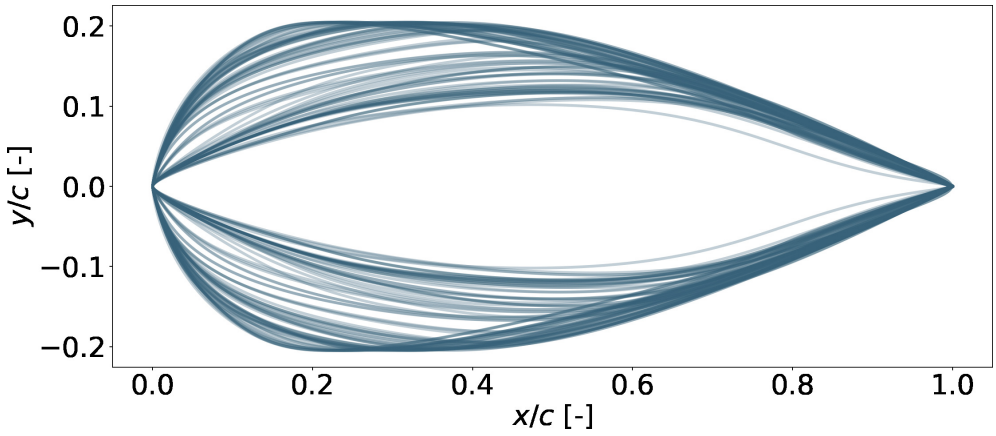

Figure 4.3: The airfoils in the Pareto front for the strut optimization stacked on top of each other.

Since the struts was used as a way to check the algorithm with a quicker objective function whether the obtained struts were of actual use was secondary. Primarily if the shape was realistic in terms of the objective functions were obtained was of interest. The struts in figure 4.3 all have an realistic airfoil shape and the set up of the algorithm was deemed to be good enough to be able to run the blade optimization without obtaining unrealistic airfoils after more costly calculations.

4.2 Blade optimization

The blade optimization as described in section 3.2.3 were also run for 200 generations and population size of 200. The full optimization run took around 9,75 hours since the AC method has inner iterations until a satisfying value for the induced velocity and the blade forces are reached and 38 angles of attack were passed to XFoil. A lot longer compared to the strut optimization but still quick considering the around 1 520 000 evaluations.

The obtained fitness value for all individuals for all generations are shown in figure 4.4. The objective functions were to maximize both w and C_P and for each generation the fitness values are in broad strokes increasing as seen by the shape created by the color change and the shape of the Pareto front. For the first generations there

are some individuals that are very far from others compared to the later generations were the individuals are closer together. The larger spread of individuals for the first generations is due to the population consisting of more individuals with relatively bad fitness values which then has a higher chance of being chosen for cross-over etc. For the later generations the GA has started to converge towards a maximum since for each generation there is a higher amount of good individuals that can be chosen since the current and previous generations individuals are in the pool of potential candidates, see section 2.4.2.1. How it converges can also be seen by the first number of individuals in a lighter blue covering a larger area compared to the later individuals in the dark blue shades that are closer together.

There is a quite sharp cut off with no individuals obtaining a higher fitness value around $C_P = 0.6$. At this cut off the C_P is very similar for several airfoils with different w. This comes from thicker airfoils producing more lift at subsonic speeds and can therefore have the same value of C_P as a thinner airfoil. Note that this C_P value is not for the whole turbine and is obtained without considering any losses. Remember that C_P is a ratio of the power extracted over the energy available in the wind and that there is a limit on how much power can be extracted. The dashed vertical line located at $C_P = 0.633$ is an ideal value obtained in a previous study by Madsen [23] with more idealized conditions. That no individuals are above this line is good validation that the obtained airfoils are reasonable.

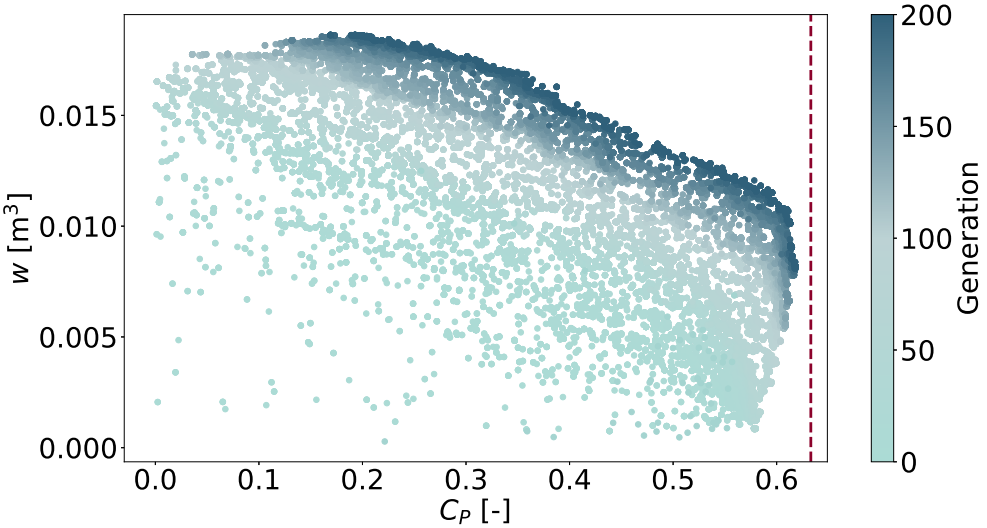

Figure 4.4: The obtained fitness values of all ≈ 40 000 individuals from one blade optimization run. The first generations are in a light blue color which gradually changes to a dark blue for the later generations. The dashed vertical line is an ideal C_P obtained with the AC method with uniform normal loading [23].

The individuals that make up the wanted optimized family of airfoils are those that are part of the Pareto front in figure 4.5, which are all the non-dominated values from 4.4 and therefore follows the same shape as the edge of the cluster. The cut off for around $C_P = 0.6$ can also be seen here with a sharp change in the shape

of the front. The front covers quite a wide range of C_P but all of them are not of the same interest since it is not desirable to lower the performance of the turbine. The individuals at the edges of the front, i.e. the individuals with either highest w or C_P, are more clumped together compared to the individuals within the front. This shows the limits of the individuals the algorithm can find with regards to the objective functions and improvement at the edges is harder to achieve and thus only a minor change is possible. Especially for the individuals with high C_P, there is much to gain in terms of w with just a small decrease in C_P.

NACA 0018 is a widely used airfoil due to its good aerodynamic performance. Evaluated with the objective functions for the blade optimization its fitness values are $C_P \approx 0.5788$ and $w \approx 0.0026$. To compare the obtained Pareto front against a well known airfoil and obtain some understanding of how it fares against what is available, NACA 0018 is also added in figure 4.5. NACA 0018 has a good value of C_P but in comparison in has a very low value of w.

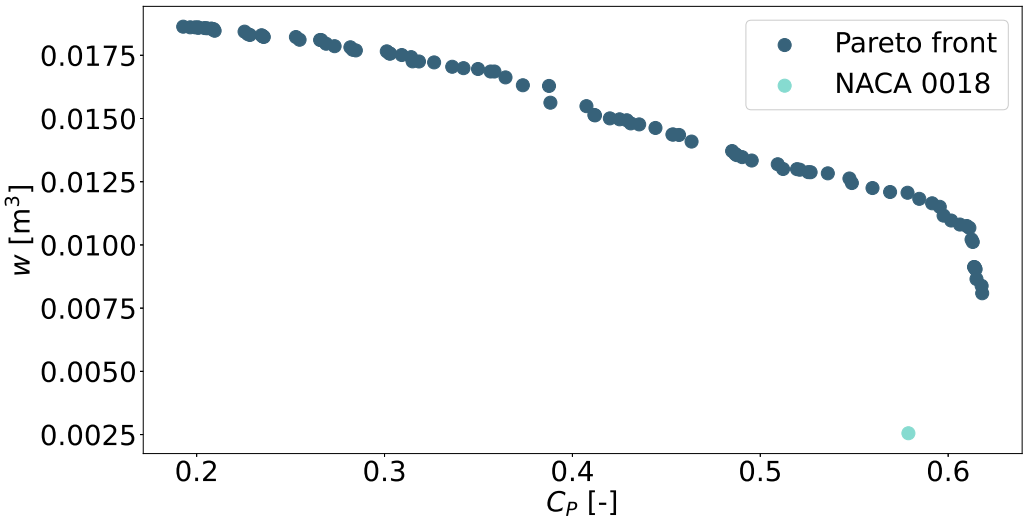

Figure 4.5: The obtained Pareto front consisting of 91 individuals with NACA 0018 added for comparison.

The airfoils that make up the Pareto front in figure 4.6 have variations in shape but there are overarching trends in the shape. Each airfoil can be seen separately in appendix A.2. The overarching trends seems to be that they are quite thick with a slightly curved outward top side, a more curved inward bottom side and a very thin part leading to a wider leading edge. As mentioned in section 2.2 the camber can be on both sides of the airfoil depending on for which azimuth angles the performance should be improved. The Pareto front airfoils all show a camber towards their top side which means an improved performance for a positive angle of attack which is during the upwind part of the rotation. The thickest part is located quite in the front of the airfoil which helps with the recovery of the flow over the airfoil. The thickest point of the airfoils is not symmetrical over the x-axis with the thickest point being further towards the leading edge for the top.

At the trailing edge many of the airfoils have sort of a flap, a sudden widening of the cross section of the trailing edge. This could increase the lift of the airfoil but it also gives an increased drag. The thickness of the airfoil towards the trailing edge seems unreasonable thin and is probably a result of the wide flap created at the trailing edge. Since the leading edges height is constrained, see table 3.2, the flap can not be created unless the airfoil becomes thinner before. Since XFoil under-estimates drag and over-estimates lift as well as not capturing base drag, as discussed in section 2.5, the flaps at the trailing edge is likely not as good as XFoil has calculated and should not be as dominant in the Pareto family as they are. It could either be that they should be smaller or not present at all. Further investigation of how much the flap impacts the drag it gives against the lift it produces is needed to understand wether or not the flaps are useful.

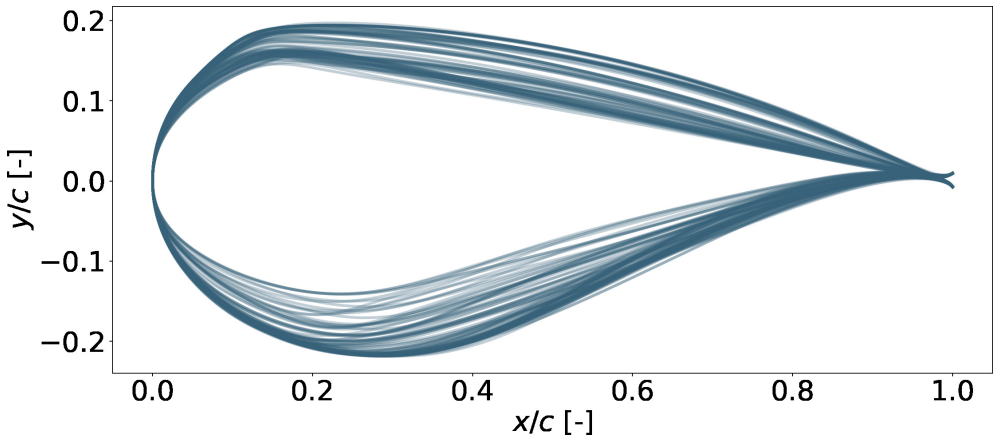

Figure 4.6: Obtained airfoils in the Pareto front stacked on top of each other.

4.2.1 Blade performance

Only two airfoils are studied: the airfoil with the same C_P as the NACA 0018 and the airfoil with maximum C_P. These are called ST 1 and ST 2 respectively. These wore chosen since it is interesting to compare with the well used NACA 0018 as well as study how the airfoil with highest C_P performs. The blade performance was calculated using XFoil with the same parameters for all three airfoils to obtain a fair comparison.

These were two of the airfoils that best fulfilled the objective functions and how their fitness values compare to the fitness values of the NACA 0018 is of interest. The ST airfoils were chosen for their C_P which together with the section modulus and thickness is presented in table 4.1. The C_P values are very similar for all of the airfoils but there is a large difference in w and also t/c between the NACA 0018 and

the ST airfoils. This is where ST airfoils better fulfill the optimization goal and why the NACA 0018 is not part of the Pareto airfoils despite having a good C_P.

Table 4.1: The obtained values of C_P and w for ST 1, ST 2 and NACA 0018.

Airfoil	C_P	w	t/c
ST 1	0.5784	0.0121	0.3401
ST 2	0.6181	0.0081	0.3080
NACA 0018	0.5789	0.0026	0.1800

As mentioned, the shape of the airfoil greatly impacts its performance. To get a visual understanding of their difference, ST 1 and ST 2 are plotted against NACA 0018 in figure 4.7. Apart from the obvious that the NACA 0018 is symmetrical whereas the ST profiles are not, the ST profiles are much thicker and follows the overarching shape trends of the Pareto front. They are unsymmetrical with a very distinct shape, a straight upper part from the thickest point towards the trailing edge as well as a camber towards the top side. The thickest points at the top and bottom are located at different x/c. Near the trailing edge the flap is also present. The biggest difference between the ST airfoils is that ST 2 is the thinner one which would give it a better aerodynamic performance and thus better C_P. The difference in thickness comes mainly from the bottom side of the airfoil.

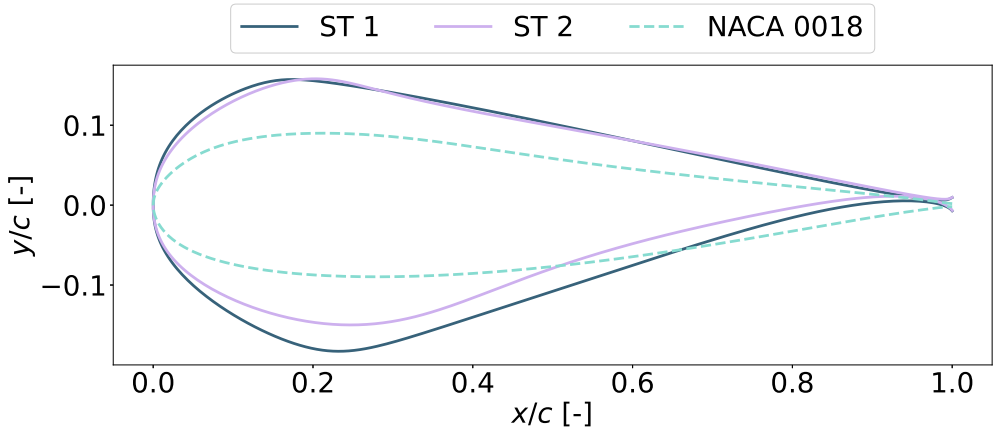

Figure 4.7: Schematic of the ST1, ST2 and the NACA 0018.

The airfoils in the family of optimized airfoils have a very distinct shape and the camber of the ST 1 is further studied a bit. The airfoils has a camber towards the top side which usually means that the camber line bends upwards, see figure 2.1, but for ST 1 the camber line goes first downward as if the concave camber was towards the bottom. That the camber line goes towards the same side as the camber is unusual. The camber line also changes curvature direction two times with first a slight curve upward, similarly to an airfoil with camber for a positive angle of attack but then it

curves downward similarly to an airfoil with a camber for negative angle of attack. Finally it curves upward again towards the trailing edge. Since there is not much of a shape difference between ST 1 and ST 2, more or less only a change in thickness, the camber line for ST 2 is thought to bo following the same overall shape. To better understand where the increased performance of the optimized airfoil family comes from the two airfoils polars are further studied.

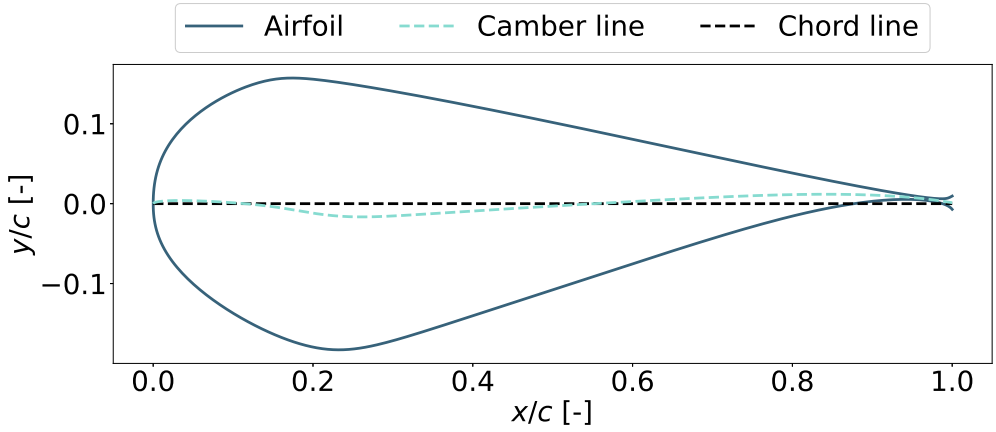

Figure 4.8: The camber line in light blue and the chord line in black of the ST 1 airfoil in dark blue.

The lift curve for a wide range of angle of attack in figure 4.9 shows a good lift for about $-8° < \alpha < 14°$ for both airfoils compared to the NACA 0018. For positive angles of attack the both ST airfoil have a higher lift than NACA 0018 but for angles of attack below around $-2°$ only ST 1 has a higher lift with ST 2 having the lowest lift. Both ST airfoils have a small amount of lift at $\alpha = 0$ as is typical for a cambered airfoil with the lift depending on the amount of camber. There is a larger increase in the amount of lift produced for the ST airfoils compared to NACA 0018 for angles of attack above 7° until about $\alpha = 16°$. The ST 1 and ST 2 has the same slope for about $-8° < \alpha < 14°$ with curve for ST 2 always being above ST 1.

Above angles of attack of 15° for all three airfoils and below angles of attack of $-8°$ for the ST airfoils there is a sudden drop in the lift produced. This change in C_l is probably due to the airfoil stalling. Though there is a great difference in the harshness of the stall with it being much more mild for the negative angles of attack compared to positive angles of attack. Since XFoil is not very good at capturing stall this is only an indication of where and to what degree stall can occur. Further shown by the much more sharp curves.

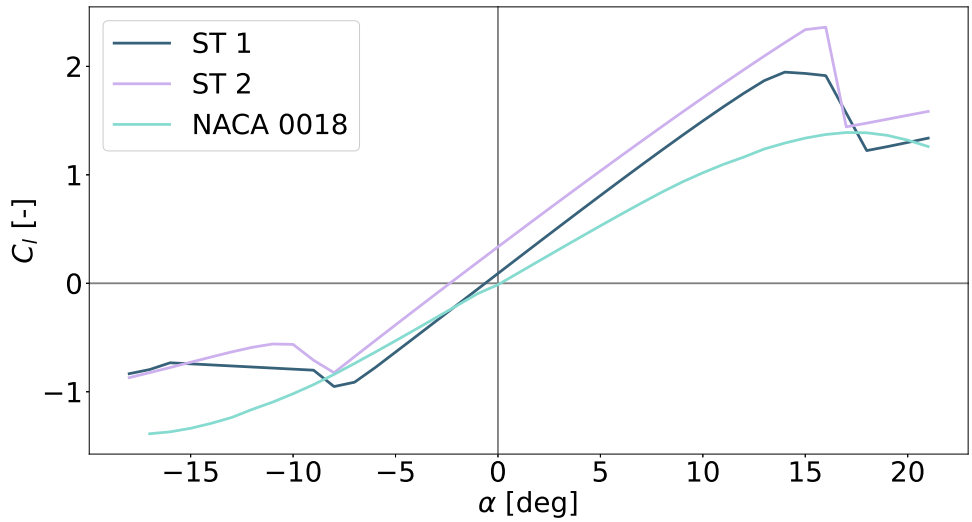

Figure 4.9: Lift curve for the ST 1, ST 2 and NACA 0018 obtained with XFoil.

The drag for all three airfoils in figure 4.10 is similar and small but not unreasonable low for $-8° < \alpha < 14°$. For angles of attack below these values and especially for those above the drag increases drastically. The airfoils should clearly not operate for angles of attack above 17° since this would greatly increase the drag. The lesser sharp drag for negative angles of attack does not give as big an increase and in the same way the lift was not greatly decreased either.

This increase in drag is due to the airfoil stalling which could be seen by the decrease in lift in figure 4.9. With a harsher stall giving a sharper increase in drag compared to the milder stall.

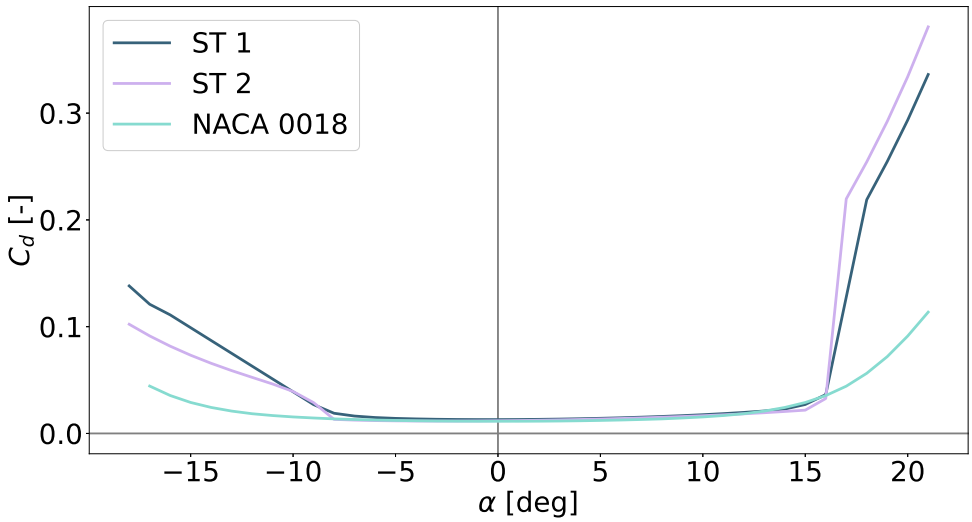

Figure 4.10: Drag curve for the ST 1, ST 2 and NACA 0018 obtained with XFoil.

One measure of efficiency is how much lift an airfoil produces compared to drag, expressed as C_l/C_d [24]. The ST airfoils are compared to NACA 0018 in figure 4.11 to get some sort of context for how much their performance have increased. ST 2 has the highest ratio for the whole range of positive angles of attack and worse for some negative angles of attack. ST 1 has a similar performance for $-5° < \alpha < 0°$ and then dips down to a worse performance down to $\alpha = -18°$ compared to the NACA 0018. For negative angle of attack the NACA 0018 has the highest lift-to-drag ratio.

The ST airfoils both have higher lift-to-drag ratio compared to the NACA 0018 for positive angles of attack and lower absolute lift-to-drag ratio which seems to indicate that favouring power production for the upwind part of the rotation is preferable. As mentioned, lift and drag vary with angle of attack and having an airfoil that performs optimally for all angles of attack is not reasonable. Instead there is a trade-off for which angle of attack the design improves the performance. The increase in performance for positive angles of attack comes at the cost of a decreased performance for negative angles of attack.

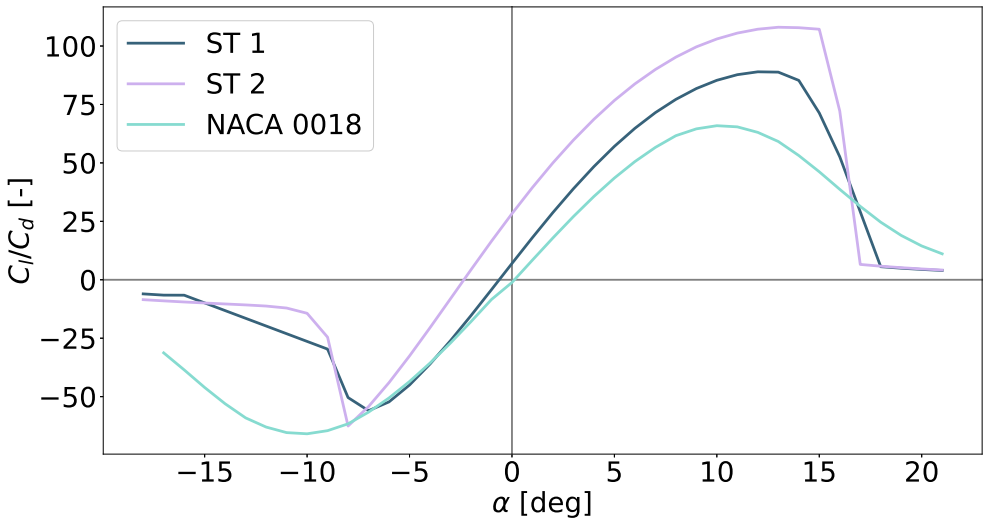

Figure 4.11: Lift-to-drag ratio for the ST 1, ST 2 and NACA 0018 obtained from XFoil

4.2.2 Turbine performance

The airfoils were optimized for a VAWT and to better grasp why these are part of an optimal airfoil family the performance of the turbine with the ST 1, ST 2 and NACA 0018 is studied. Remember that the airfoil in a VAWT operates with varying angles of attack during a full rotation with positive angle of attack for the upwind part and negative angle of attack for the downwind part, see section 2.2 for more details. The turbine performance was calculated for all three airfoils with the AC method with the same parameters in XFoil and for the turbine with $\lambda = 3$ and the same range $-18° < \alpha < 22°$ as input to XFoil to get a fair comparison.

The three airfoils overall operate at similar angles of attack for one rotation of the turbine in figure 4.12. The NACA 0018 operates at highest absolute angle of attack for both the upwind and downwind region of the rotation. The ST 1 operates at higher angle of attack compared to the ST 2 airfoil for positive angle of attack and they operate at more or less the same angle of attack for the negative angle of attack. While there is not much difference between their maximum angle of attack it could have a large impact on the performance since maximum lift occurs at higher angle of attack followed by stall. It is preferable therefore to have an airfoil that can produce the same lift for a lower angle of attack.

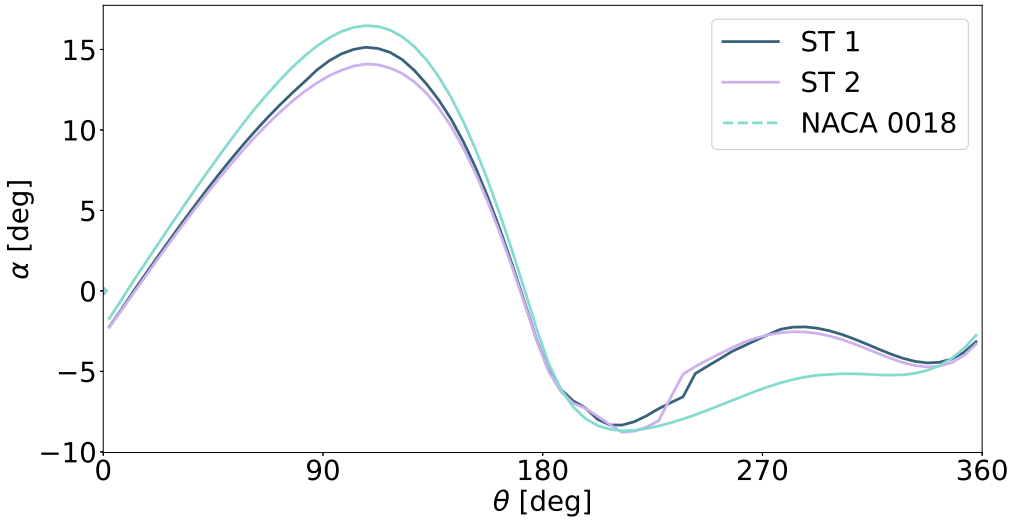

Figure 4.12: The angles of attack for the ST 1, ST 2 and NACA 0018 during a full rotation of the VAWT. The angle of attack was calculated with the AC method.

The lift coefficient in figure 4.9 shows how the three airfoils perform different for a full rotation of the turbine. For the upwind region the ST 2 airfoils produces the most amount of lift followed by the ST 1 airfoil. It is clear how the design of the ST airfoils performs better at positive angles of attack. The design prioritises the undisturbed flow during the upwind region compared to the downwind region. The lift for the NACA 0018 is more even for a full rotation in comparison.

For the upwind part the lift force is directed inwards but during the downwind region the lift force is directed outward and is then in the same direction as the inertial forces and thus a higher bending moment is inflicted on the blade. Decreasing the lift force at these angle of attack is beneficial in that sense. The downwind region is also where the least amount of energy can be extracted since energy has already been extracted from the blades during the upwind part.

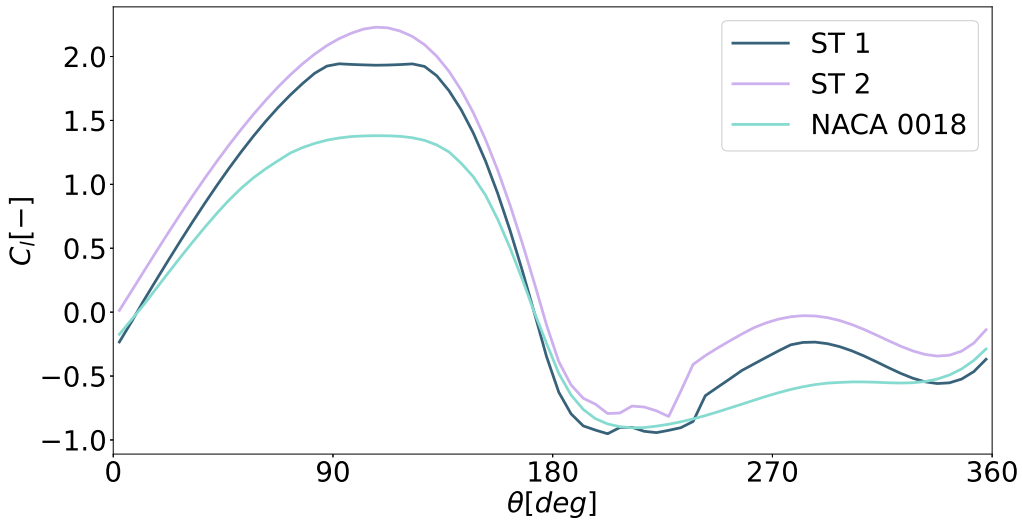

Figure 4.13: Lift coefficient for one full rotation of the VAWT. C_l was obtained with the AC method.

The drag in figure 4.14 is very different for the three airfoils shortly after $\theta = 90°$. The NACA 0018 has a comparably high drag which can also be seen in figure 4.10 with an increase in drag starting at $\alpha \approx 15°$. Since the NACA 0018 operate at a slightly higher angle of attack it enters the area where it starts to stall for $\alpha > 15°$. The ST 2 has a lower drag compared to both the NACA 0018 and ST 1 for almost the full rotation whereas the ST 1 airfoil has a lower drag for positive angle of attack and a larger drag for negative azimuth compared to the NACA 0018. For the negative azimuth the higher drag for ST 1 is compensated for by the higher lift in figure 4.9.

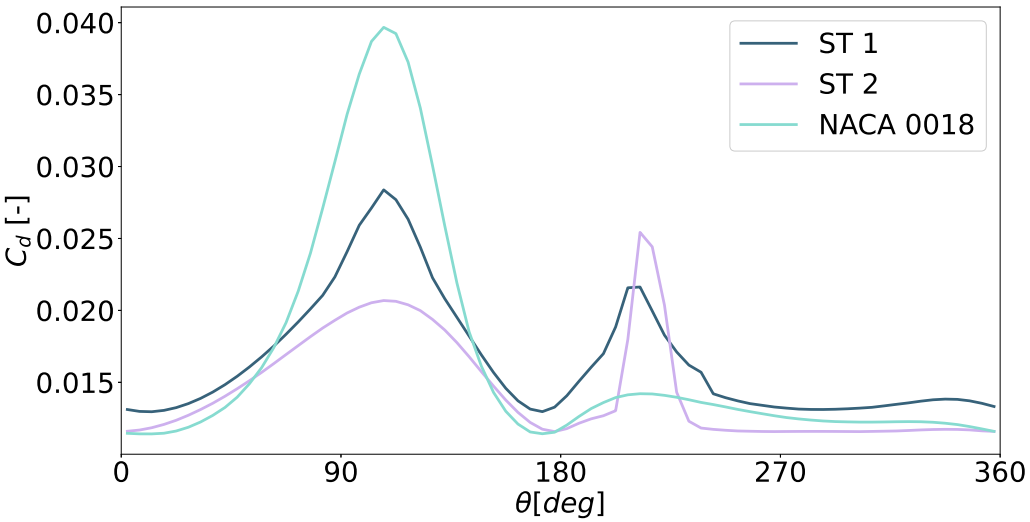

Figure 4.14: Drag coefficient for one full rotation of the VAWT. C_d was obtained with the AC method.

4.2.3 Alternative Reynolds number

The blade optimization was also run with Reynolds number set to $5 \cdot 10^6$. An altered Re number should impact the performance of the airfoil since it gives a different flow condition. The set up described in section 3.2.3 was un-altered except for the Reynolds number which was set to $Re = 5 \cdot 10^6$.

The fitness values for all evaluated individuals from the optimization are shown in figure 4.15. It shares a lot of similar features to figure 4.4 in terms of how the fitness values improves for the population from one generation to the next. Though, there seems to be almost two fronts. One being the Pareto front which has almost the same value of w until $C_P \approx 0.63$ where it instead starts following the same value of C_P but with decreasing w. That there is no trade-off between w and C_P for that many individuals is unrealistic. Also considering that the front goes past the value of the idealized C_P is one more reason to be sceptical of the validity of the Pareto front. The other front is following the grey individuals located below the small gap in the darker blue area. This front is much more similar to the Pareto front in figure 4.5. It seems that XFoil cannot properly calculate the w and C_P with the increased Reynolds number. The reason for this could not be properly investigated and therefore a better result were not obtained.

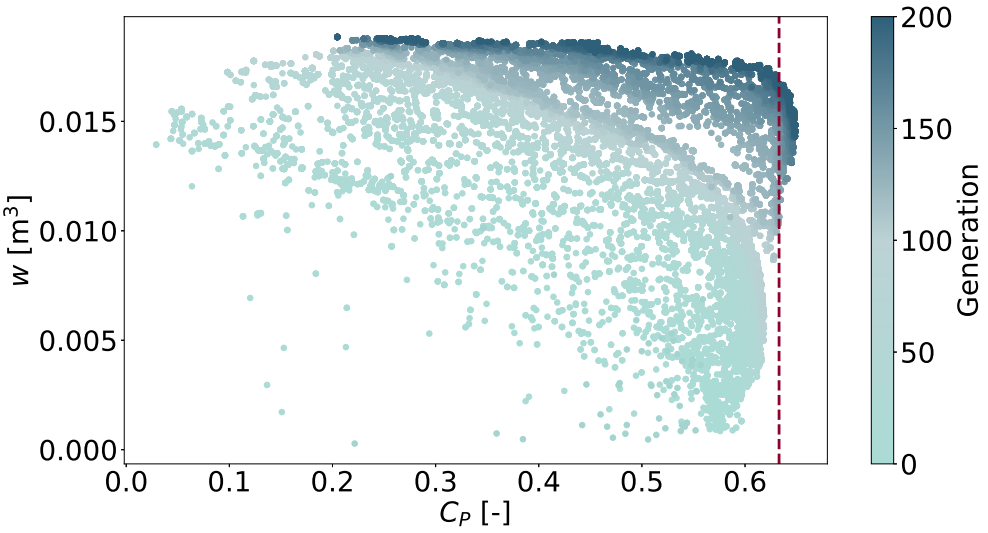

Figure 4.15: The values of C_P and w for all evaluated individuals for the blade optimization. The first generation are shown in dark blue which gradually goes to red for the latest generation. The dashed vertical line is an ideal C_P obtained from the AC method with uniform normal loading [23].

The airfoils that make up the Pareto front are shown in figure 4.16. The overarching shapes are still following the same trend as with $Re = 1 \cdot 10^6$. Though there is not much change in the thickness which is expected since almost the whole Pareto front has the same w. The thickest part at the bottom seems to have a quite sharp change in curvature which leads to the over-estimated turbine performance.

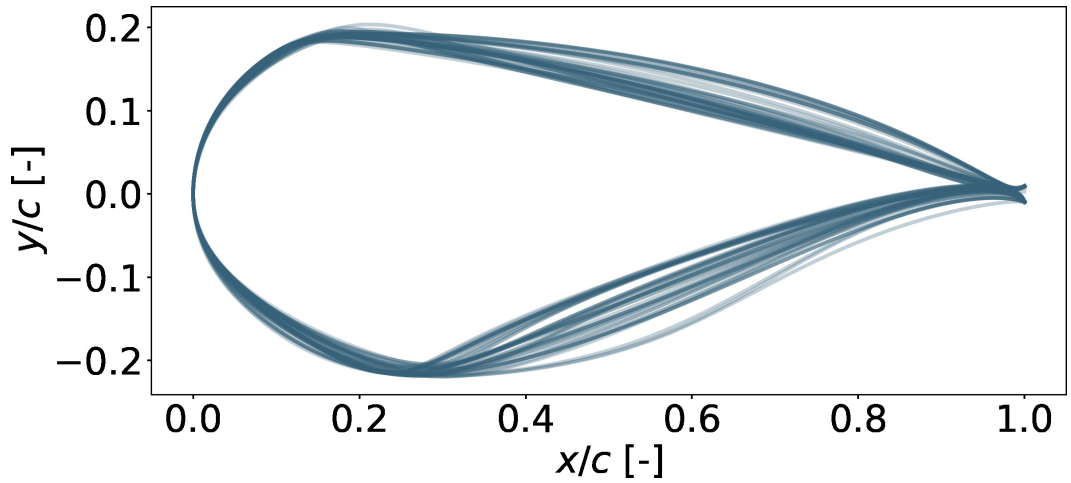

Figure 4.16: All airfoils in the Pareto front stacked.

4.3 Comparison to CFD

To validate the accuracy of the results obtained, the NACA 0012 and NACA 0040 were simulated with CFD at $Re = 5 \cdot 10^6$ with the Spalart-Allmaras turbulence model. All airfoils in the family of optimized airfoils fall within the range between NACA 0012 and NACA 0040 in terms of thickness. While the impact of a camber is not covered by this comparison the variation in thickness gives at least some validation for the range of optimized airfoils. They were run for a single angle of attack and for the same flow parameters in both SU2 and XFoil. From both graphs the difference in lift and drag coefficient does not differ much and is almost the same for the thin NACA 0012 but it is a 17% difference in the lift coefficient and a 7.9% difference in the drag coefficient for NACA 0040. This shows the good quality of the polars obtained from XFoil and its ability to capture trends related to thickness.

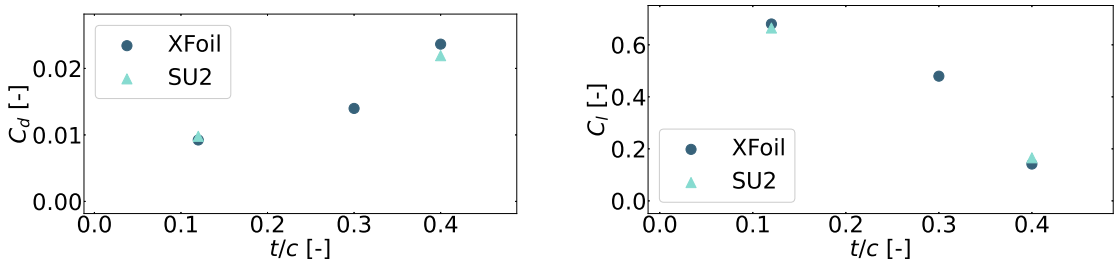

(a) Value of C_d **(b)** Value of C_l

Figure 4.17: Difference between XFoil and SU2 calculated lift and drag coefficient calculated at $Re = 5 \cdot 10^6$ at 6° angle of attack for three different NACA profiles.

5
Conclusion

The aim of this thesis was to find the optimized family of airfoils for a VAWT along a Pareto curve for a 2D airfoil profile with regards to the section modulus and the power coefficient. Conclusions about the optimized family of airfoils, their potential gain and suggestions for future work are presented.

5.1 Optimized family of airfoils

A family of optimized airfoils was obtained through bi-objective optimization with an aerodynamic and a structural objective. The family of optimized airfoils indicates to be able to have good performance when used in a VAWT. Though it was assumed that there were no losses which gives an idealized C_P. With losses the C_P will be lower [23] and give a better indication for the performance of the turbine.

The obtained family of airfoils all had a flap towards the trailing edge which might not contribute to an increased performance as much as XFoil has calculated, hence there is a slight uncertainty in the calculated increase in performance. The flap increases lift but it also increases drag which could be underestimated. Therefore, further simulations are needed to determine if the flap should be as it is, of smaller size or not there at all. It is not deemed that the overall shape of the family of airfoils are unreasonable and is very interesting. Though, changing the flap could mean slight changes the shape but not probably not anything that would drastically change the overall shape. Using CFD should be able to answer theses questions of the flap and the impact a change of it would have on the overall shape.

Two specific airfoils from the family were further studied: ST 1 and ST 2. ST 1 has the same C_P as the NACA 0018 and the ST 2 has the highest C_P of the optimized family. When studying the airfoil and turbine performance of ST 1 and ST 2 there are some interesting possibilities in increased performance. Since the VAWT rotates there is a difference in the energy of the flow for the upwind and downwind part. The blade extracts kinetic energy from the upwind region and therefore there is less energy that can extracted during the downwind region of the rotation. Both airfoils favour power production for the upwind part of the rotation rather than the downwind part. Overall there is an increase in the performance of the ST airfoils with it compensating for the worse performance during the downwind region with a larger increase in the performance for the upwind region. No conclusion could be made about the sensitivity to the Reynolds number.

5.2 Possibility to lower the weight of the blades

Using the obtained airfoil ST 1 has the potential to save weight on the blades compared to using the NACA 0018. They both have very similar C_P but a large difference in thickness and section modulus in table 4.1. If the blades are required to have a certain value of the section modulus an airfoil profile with a higher w does potentially not need extra material to be able to withstand the stress and bending of the blade as mentioned in section 2.2.1. To get a rough estimate of how much weight the ST 1 would save compare to the NACA 0018 some short calculations were made to obtain a rough estimate.

It is assumed that the spar caps are straight thin walled rectangles located completely opposite of each other and that the load is fully taken by those. The section modulus is calculated according to equation 2.4 but for a thin walled rectangle it is simply its width, b, times its wall thickness, t, and the distance between the walls, d, and becomes

$$w = b \cdot t \cdot d. \tag{5.1}$$

From equation 5.1 it is possible to see that $w \propto d$ which gives $m \propto 1/d$. In table 4.7 the difference in thickness between ST 1 and NACA 0018 is a factor of about 1.9. If ST 1 were used as a profile for the blade the weight would be about halved.

Even if it is an estimate it is still interesting to have an indication of the potential weight loss with a ST airfoil.

5.3 Future work

To further improve on this work and gain a more accurate family of optimized airfoils there are a few suggestions that could help with obtaining that. The assumptions and limitations that have been set would also gain from being studied.

The optimization has only been run with XFoil which as stated in section 2.5 is a panel method based on potential flow and can not capture phenomena such as re-circulation. It also overestimates lift and underestimates drag and the obtained family can be assumed to be optimized with these limitations. To improve on the design and obtain an airfoil profile with better lift and drag properties, the obtained family of optimized airfoils could be used as a starting guess when using CFD. Based on work that could not be presented in this thesis, SU2 would be a good fit together with a gradient-based optimization algorithm. Mesh deformation and mesh adaptation is implemented in SU2 which means that a new mesh does not have to be regenerated for each change in the airfoil shape.

The simulations have only been run in 2D and can therefore not accurately capture stall since that requires simulations done in 3D. Due to the high computation cost this was not possible to be part of the thesis. Though, to accurately evaluate the performance of the airfoil stall must be considered since it greatly effects lift and

drag of the airfoil. Since the airfoils operates close to where it stalls as seen in 4.12 and 4.9 it might be that it actually does operate during stall for the negative angle of attack. Even if the stall in this region in figure 4.9 is quite light it still impacts the airfoils ability to produce lift.

Unsteady airfoil aerodynamics have not been taken into account for this work. An optimized airfoil profile including these effects would ensure a better turbine performance.

The tip speed ratio impacts the optimum performance of the turbine and it might be interesting to study for which TSR an airfoil performs optimally at.

Bibliography

[1] O. Ellabban, H. Abu-Rub, and F. Blaabjerg, "Renewable energy resources: Current status, future prospects and their enabling technology," *Renewable and Sustainable Energy Reviews*, vol. 39, pp. 748–764, 2014, ISSN: 1364-0321. DOI: https://doi.org/10.1016/j.rser.2014.07.113.

[2] A. Henderson, M. Collu, and M. Masciola, "Overview of floating offshore wind technologies," in *Floating Offshore Wind Energy*, J. Cruz and M. Atcheson, Eds., Springer Cham, 2016, pp. 87–130, ISBN: 978-3-319-29396-7. DOI: https://doi.org/10.1007/978-3-319-29398-1.

[3] B. Hand, G. Kelly, and A. Cashman, "Aerodynamic design and performance parameters of a lift-type vertical axis wind turbine: A comprehensive review," *Renewable and Sustainable Energy Reviews*, vol. 139, Jan. 9, 2021. DOI: 10.1016/j.rser.2020.110699.

[4] C. Liang and H. Li, "Aerofoil optimization for improving the power performance of a vertical axis wind turbine using multiple streamtube model and genetic algorithm," *Royal Society Open Science*, vol. 5, no. 7, Jul. 2018. DOI: 10.1098/rsos.180540.

[5] C. S. Ferreira and B. Geurts, "Aerofoil optimization for vertical-axis wind turbines," *Wind energy*, vol. 18, pp. 1333–1514, 8 2015. DOI: https://doi.org/10.1002/we.1762.

[6] R. Kemp, "Airfoil optimization for vertical axis wind turbines," Mar. 13, 2015.

[7] H. Babinsky, "How do wings work?," vol. 38, Nov. 2003.

[8] J. Manwell, J. McGowan, and A. Rogers, *Wind energy explained, Theory, Design and Application*, 2nd ed. John Wiley & Sons Ltd, 2009, ISBN: 978-0-470-01500-1.

[9] "Lab 10: Wing structural analysis and bending test," in *Unified Engineering*, MIT OpenCourseWare, Cambridge MA, 2005. [Online]. Available: https://ocw.mit.edu/courses/16-01-unified-engineering-i-ii-iii-iv-fall-2005-spring-2006/resources/spl10b/.

[10] H. A. Madsen, "On the ideal and real energy conversion in a straight bladed veritcal axis wind turbine," Ph.D. dissertation, Aalborg University Centre, 1983. DOI: http://dx.doi.org/10.13140/RG.2.1.3036.5929.

[11] Z. Cheng, H. Madsen, Z. Gao, and T. Moan, "Aerodynamic modeling of floating vertical axis wind turbines using the actuator cylinder flow method," *Energy Procedia*, vol. 94, pp. 531–543, Sep. 2016. DOI: 10.1016/j.egypro.2016.09.232.

[12] C. S. Ferreira, H. A. Madsen, M. Barone, B. Roscher, P. Deglaire, and I. Arduin, "Comparison of aerodynamic models for vertical axis wind turbines,"

Journal of Physics: Conference Series, vol. 524, p. 012 125, Jun. 2014. DOI: 10.1088/1742-6596/524/1/012125.

[13] K. Giannakoglou, "Design of optimal aerodynamic shapes using stochastic optimization methods and computational intelligence," *Progress in Aerospace Sciences*, vol. 38, no. 1, pp. 43–76, 2002. DOI: https://doi.org/10.1016/S0376-0421(01)00019-7.

[14] K. Deb, S. Agrawal, A. Pratap, and T. Meyarivan, "A fast and elitist multiobjective genetic algorithm: Nsga-ii," *IEEE Trans. Evol. Comput.*, vol. 6, pp. 182–197, 2002.

[15] M. Wahde, *Biologically Inspired Optimization Methods - An Introduction*. WIT press, 2008, ISBN: 978-1-84564-148-1.

[16] J. Blank and K. Deb, "Pymoo: Multi-objective optimization in python," *IEEE Access*, vol. 8, pp. 89 497–89 509, 2020.

[17] M. Drela, "XFOIL: An analysis and design system for low reynolds number airfoils," in *Low Reynolds Number Aerodynamics*, T. J. Mueller, Ed., Berlin, Heidelberg: Springer Berlin Heidelberg, 1989, pp. 1–12, ISBN: 978-3-642-84010-4. DOI: $10.1007/978-3-642-84010-4_1$.

[18] E. Adler, A. Christison Gray, and J. Martins, "To cfd or not to cfd? comparing rans and viscous panel methods for airfoil shape optimization," Sep. 2022.

[19] A. Aihara, V. Mendoza, A. Goude, and H. Bernhoff, "Comparison of three-dimensional numerical methods for modeling of strut effect on the performance of a vertical axis wind turbine," *Energies*, vol. 15, no. 7, p. 2361, Mar. 2022. DOI: 10.3390/en15072361. [Online]. Available: https://doi.org/10.3390/en15072361.

[20] A. Björck, "Coordinates and calculations for the FFA-W1-xxx, FFA-W2-xxx and FFA-W3-xxx series of airfoils for horizontal axis wind turbines," The Aeronautical Research Institute of Sweden, Tech. Rep., 1990.

[21] W. A. Timmer and R. P. J. O. M. van Rooij, "Summary of the delft university wind turbine dedicated airfoils," *Journal of Solar Energy Engineering*, vol. 125, no. 4, pp. 488–496, Nov. 2003. DOI: 10.1115/1.1626129. [Online]. Available: https://doi.org/10.1115/1.1626129.

[22] G. Ramanujam, H. Özdemir, and H. W. M. Hoeijmakers, "Improving airfoil drag prediction," *Journal of Aircraft*, vol. 53, no. 6, pp. 1844–1852, 2016. DOI: 10.2514/1.C033788. eprint: https://doi.org/10.2514/1.C033788.

[23] H. A. Madsen, U. S. Paulsen, and L. Vitae, "Analysis of vawt aerodynamics and design using the actuator cylinder flow model," *Journal of Physics: Conference Series*, vol. 555, no. 1, Dec. 2014. DOI: 10.1088/1742-6596/555/1/012065.

[24] S. Gudmundsson, "Chapter 8 - the anatomy of the airfoil," in *General Aviation Aircraft Design*, S. Gudmundsson, Ed., Second Edition, Butterworth-Heinemann, 2022, pp. 257–319, ISBN: 978-0-12-818465-3. DOI: https://doi.org/10.1016/B978-0-12-818465-3.00008-2.

A

Appendix 1

A.1 Known airfoils in initial generation

The initial generation consists in part of the known airfoils in table A.1.

Table A.1: Known airfoils in the initial generation. Some were also used as an inverted version.

DF 101	DU 06-W-200 VAWT
Falcon	FFA - W3 - 211
FFA-W3-241	FFA-W3-270blend
FFA-W3-301	HAM-STD HS1-708
HAM-STD HS1-712	NACA 2-H-15
NACA 5-H-20	NACA 63(23)-215 MOD B
NACA 64-008A	NACA 64A210
NACA 2415	NACA M2
NACA 0006	NACA 0012
NACA 0016	NACA 0018
NACA 0020	NACA 0024
NACA 0032	NACA 0040
NACA 2212	NACA 2414
NACA 2416	NACA 3212
NACA 3215	NACA 3416
NACA 4212	NACA 6409 9%
NASA SC(2)-0010	NASA SC(2)-0012
NASA SC(2)-0518	ONERA HOR07
ONERA HOR12	ONERA HOR20
RAE 100	RAE 2822
SP4621HR	

A.2 Family of optimized blade profiles

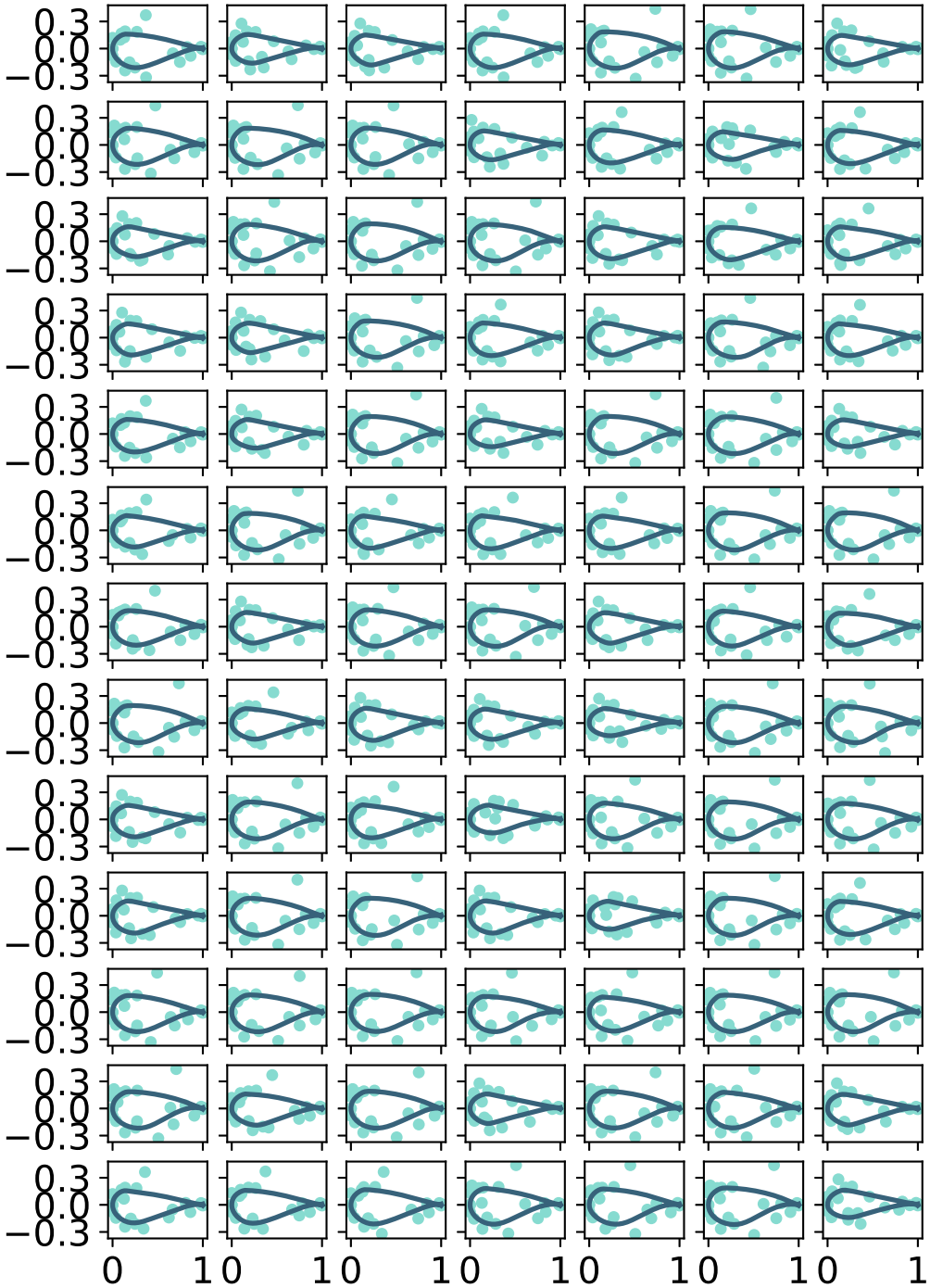

Figure A.1: Every airfoil in the obtained family of optimized airfoils.

DEPARTMENT OF MECHANICS AND MARITIME SCIENCES
CHALMERS UNIVERSITY OF TECHNOLOGY
Gothenburg, Sweden
www.chalmers.se

CHALMERS
UNIVERSITY OF TECHNOLOGY